Journal of Analytical and Applied Pyrolysis 193 (2026) 107477

Contents lists available at ScienceDirect

Journal of Analytical and Applied Pyrolysis

journal homepage: www.elsevier.com/locate/jaap

A comprehensive kinetic study of hemicellulose pyrolysis: TGA datasets and detailed quantitative speciation for xylan, glucomannan and arabinoxylan

Eleonora Benedetto [a], Veronica Piazza [a], Luca Lietti [a], Alessio Frassoldati [b], Tiziano Faravelli [b], Alessandra Beretta [a,*]

[a] Laboratory of Catalysis and Catalytic Processes, Dipartimento di Energia, Politecnico di Milano, via La Masa 34, Milano 20156, Italy
[b] CRECK Modeling group, Dipartimento di Chimica, Materiali e Ingegneria Chimica, Politecnico di Milano, Piazza Leonardo da Vinci 32, Milano 20133, Italy

ARTICLE INFO

Keywords:
Pyrolysis
Hemicellulose
TGA
Kinetic modeling
Biomass conversion
Speciation

ABSTRACT

This study investigates the thermal decomposition and product distribution of three representative hemicellulose polysaccharides: xylan (hardwoods), glucomannan (softwoods), and arabinoxylan (herbaceous biomass) to obtain data aimed at the development of accurate kinetic models. A novel thermogravimetric analysis (TGA) based methodology, previously developed for cellulose, was applied, integrating kinetic analysis with detailed online and offline product speciation at multiple heating rates (3–100 °C/min). Results revealed distinct devolatilization patterns among the hemicelluloses. While xylan exhibited a two-step decomposition with significant gas formation, glucomannan displayed a single sharp degradation peak, yielding the highest bio-oil fraction. Arabinoxylan showed yields more distributed among the different product categories, with bio-oil characterized by high anhydrosugars formation. Online mass spectrometry (MS) analysis identified CO, CO_2, CH_4, and H_2O evolution closely linked to thermal degradation pathways. Quantitative gas chromatography (GC-MS/FID) analysis of bio-oil unveiled diverse product distributions: xylan primarily formed ketones and furanic compounds, glucomannan produced C_6 anhydrosugars, and arabinoxylan yielded significant C_5 sugar derivatives. Comparison with lumped kinetic models for hemicellulose pyrolysis highlighted substantial discrepancies, particularly in bio-oil composition and water mass yield, underscoring the need for refined reaction pathways. The high-quality dataset presented in this study provides significant insights into hemicellulose pyrolysis kinetics, enabling the improvement of predictive models for biomass thermochemical conversion.

1. Introduction

In the last decades, the growing need for sustainable energy solutions has promoted the exploration of alternatives to conventional fossil-based feedstocks, such as lignocellulosic and waste biomass [1–4], a renewable and versatile resource, which holds significant promise as a feedstock for producing biofuels, biochemicals, and energy carriers.

Bioenergy currently accounts for 55 % of renewable energy and 6 % of the global energy supply, and it has seen a steady growth of 3 % annually from 2010 to 2022 [5,6]. However, to meet the International Energy Agency's Net Zero Emissions (NZE) scenario for 2050, its growth rate needs to accelerate to 8 % annually, already by 2030 [5,7].

Pyrolysis, a thermochemical process that thermally decomposes biomass in an oxygen-free environment, stands out as a versatile and promising technology for biomass valorization. It produces three main product streams: a gaseous fraction containing compounds like CO, CO_2, H_2, and CH_4; a liquid bio-oil composed of oxygenated species; and a solid carbon-rich residue known as biochar [8]. Despite its importance, the complex chemistry of biomass pyrolysis remains insufficiently understood, largely due to the intricate structure of lignocellulosic feedstocks [9]. Lignocellulosic biomass is constituted by three major components: cellulose, hemicellulose, and lignin. Their proportions and chemical structures vary depending on the biomass source, with smaller amounts of pectin, proteins, and minerals also present. To fully understand the thermal behavior of real biomass, it is imperative to investigate the behavior of all its constituents. Hemicellulose, a heterogeneous mixture of amorphous and partially branched polysaccharides, is one of the least explored components in literature, despite accounting for approximately 30 % of real biomass [10]. Unlike the uniform composition of cellulose, hemicellulose comprises various building blocks, including pentoses (arabinose, xylose), hexoses (glucose, galactose, mannose), hexuronic acids (glucuronic acid, galacturonic acid) and

* Corresponding author.
E-mail address: alessandra.beretta@polimi.it (A. Beretta).

https://doi.org/10.1016/j.jaap.2025.107477
Received 23 May 2025; Received in revised form 7 November 2025; Accepted 13 November 2025
Available online 14 November 2025

acetyl groups, as well as small amounts of L-rhamnose and L-fucose [11]. These functional groups can assemble into a range of various hemicellulose polysaccharides with diverse structures from linear to highly branched. The abundance and detailed structures of these hemicellulose polysaccharides vary widely, depending on the biomass sources. Hardwood biomass (e.g. deciduous trees) primarily contains xylan-based hemicelluloses, accounting for 15–30 wt% of dry biomass, with chains of β-D-xylose and side groups like 4-O-methyl-D-glucuronic acid. Typical molar ratios of xylose to glucuronic acid range from 25:1 to 4:1 [11,12]. Contrarily, in softwood species (e.g. conifers), glucomannans are the predominant hemicellulose polysaccharides accounting for 20–25 wt% of dry biomass, characterized by a backbone of β-D-mannose and β-D-glucose units. The molar ratio of mannose to glucose is approximately 3:1 [11]. Instead, herbaceous plants mostly comprise arabinoxylan, a linear chain of β-D-xylose in which L-arabinofuranosyl substituents are linked through O-2 or O-3. In this case the molar ratio of xylose to arabinose is around 5:3 [11,12].

One critical research area in biomass pyrolysis is the development of kinetic models for the devolatilization step, able to describe quantitatively and qualitatively the release and the distribution of primary vapor products from the solid biomass [9,13,14]. These primary products are the results of complex kinetics within the solid hemicellulose particle and are then released in the vapor phase. These products can then undergo secondary reactions in the vapor phase, but while the knowledge on homogeneous kinetic schemes is well established, devolatilization chemistry remains poorly understood, despite being fundamental to improve pyrolysis technologies and develop predictive modelling tools for different feedstocks. Moreover, insights into devolatilization are also crucial for related processes such as gasification and combustion, where it represents the first conversion stage.

Different strategies have been developed to model biomass pyrolysis kinetics, varying in their level of complexity and detail. Global models, such as single-step first-order reaction, n^{th}-order models and distributed activation energy model (DAEM) [15,16], describe pyrolysis as one or a few overall reactions, reproducing mass loss and apparent kinetics but without resolving product distributions. Mechanistic or network models (such as the bio-FLASHCHAIN™ [17]) attempt to describe more detailed reaction pathways, involving several reactions and intermediates; while highly informative, these models remain incomplete for biomass components and are computationally demanding [9,13,14]. Lumped kinetic models [18,19] offer a semi-detailed compromise, simplifying the complex chemistry of biomass pyrolysis by grouping many individual reactions and products into a smaller set of 'lumps' or 'pseudo-components' (e.g., ketones, aldehydes, char, water, CO_2) that share similar properties [13]. In this approach biomass is represented in terms of its main constituents (cellulose, hemicellulose, and lignin) so that the overall behavior of real feedstocks can be reconstructed as the additive, weighted contribution of each fraction [6]. This lumping technique represents an engineering approach to reduce system complexity, enabling the development of predictive models for reactor design and process optimization. Over time, lumped models have been refined, with early schemes developed by some of the authors [6,18,20–22] forming the basis for more advanced models proposed by researchers such as Dussan et al. [19] and Debiagi et al. [18]. The accuracy of these models remains closely tied to the quality of experimental data used for parameter calibration; however, the current literature still lacks comprehensive and kinetically informative datasets. To develop effective kinetic models, two types of experimental data are essential: devolatilization rates and quantitative product speciation. While several studies in literature have reported devolatilization rates [23–29], there are only a few examples of works providing quantitative product characterization. Notably, S. Niksa compiled a comprehensive hemicellulose pyrolysis database, which includes several studies resolving major gas products and illustrating the impact of secondary volatiles on product distributions [30]. Nevertheless, comprehensive quantitative characterization of both gaseous and condensable products across a range of heating rates remains limited. In particular, systematic data on hemicellulose pyrolysis with resolved condensables are still scarce, despite their importance for kinetic model development.

For this reason, developing an experimental protocol capable of delivering accurate experimental data and identifying the full range of pyrolysis products is crucial for the advancement and validation of kinetic schemes. Thermogravimetric analyzers (TGA) are widely used in biomass pyrolysis studies to investigate decomposition, mass loss, and thermal stability, often in combination with analytical tools such as gas chromatographs or mass spectrometers for detailed product characterization [29,31–35]. Building on this approach, the authors previously developed a novel TGA-based methodology that integrates kinetic analysis with comprehensive product quantification [25]. This protocol enables the identification and the quantification of the entire range of pyrolysis products – gases, condensable species and solid residual – by combining different analytical methodologies and sampling procedures, coupled with calibration protocols. The methodology was first validated through cellulose pyrolysis experiments, leading to the development of an improved kinetic scheme with refined reactions and product categories [25,36]. Then its applicability was also demonstrated for studying other biomass components, obtaining preliminary results on hemicelluloses like xylan and glucomannan [26].

The primary objective of this work is to build upon this groundwork [18,25,26,36] and to expand the investigation by delivering a comprehensive experimental dataset on the devolatilization behavior and product distribution of hemicellulose. Additionally, this study aims to critically compare the experimental results with previous lumped kinetic models, thereby underscoring the necessity of expanding experimental knowledge in biomass pyrolysis to improve model accuracy and reliability.

Three model biomasses were chosen to represent hemicellulose in the three main classes of real biomass: xylan for hardwood biomass, glucomannan for softwood biomass, and arabinoxylan for herbaceous plants [12]. Pyrolysis experiments were conducted using the TGA-based methodology described in [25]. This approach enabled the collection of intrinsic rate data together with detailed, quantitative product speciation. This work focuses on the investigation of various heating rates (3, 10, 20, 50, and 100 °C/min) and the on-line dynamic evolution of gaseous products, providing novel insights on the kinetics of hemicellulose decomposition. The experimental findings were then compared with predictions from the models by Dussan et al. and Debiagi et al. [18,19]. To the best of our knowledge, the results provide novel and valuable understanding of hemicellulose pyrolysis currently unavailable in literature.

2. Materials and methods

2.1. Materials

In this work pyrolysis experiments were performed on model biomasses purchased from Megazyme International. Three different hemicelluloses were chosen: beechwood-derived xylan, low viscosity konjac-derived glucomannan and insoluble (gel) form wheat-derived arabinoxylan.

For what concerns the monosaccharide composition, xylan was characterized by a xylose:glucuronic acid ratio of 8:1 and by a 7.8 % content of other sugar compounds, glucomannan presented a mannose: glucose ratio of 3:2 and arabinoxylan had a xylose:arabinose ratio of 2:1 and a 4.5 % content of other sugar compounds. Table 1 reports further details of these biomass constituents. The elemental composition of all biomasses was characterized using an Elemental Analyzer Costech ECS model 4010, which enabled the simultaneous determination of C and H weight percentage. The O content was calculated as the complementary fraction. The proximate analysis was carried out in a thermogravimetric analyzer (Hitachi STA7300 TG-DTA) following the ASTM method D7582–12. All samples were used without any pre-treatment for

Table 1
Biomass tested in this study.

	Xylan	Glucomannan	Arabinoxylan
Sugar composition	Xylose: 80.8 % Glucuronic acid: 11.4 % Other sugars: 7.8 %	Mannose: 60 % Glucose: 40 %	Xylose: 62 % Arabinose: 33.5 % Other sugars: 4.5 %
Molecular structure	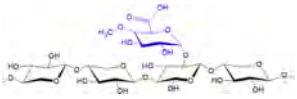	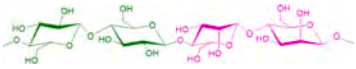	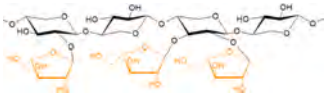
Elemental analysis	C: 40.0 ± 0.2 [wt%] H: 6.8 ± 0.2 [wt%] O: 53.3 ± 0.4 [wt%]	C: 39.0 ± 0.2 [wt%] H: 7.1 ± 0.2 [wt%] O: 53.9 ± 0.4 [wt%]	C: 47.7 ± 0.2 [wt%] H: 6.7 ± 0.2 [wt%] O: 45.6 ± 0.4 [wt%]
Proximate analysis	Moisture: 11.5 [wt%] Volatile matter: 66.3 [wt%] Fixed carbon: 18.8 [wt%] Ashes: 2.6 [wt%]	Moisture: 11.2 [wt%] Volatile matter: 71.3 [wt%] Fixed carbon: 14.9 [wt%] Ashes: 2.6 [wt%]	Moisture: 9.5 [wt%] Volatile matter: 80.7 [wt%] Fixed carbon: 9.3 [wt%] Ashes: 0.5 [wt%]

pyrolysis experiments in the TGA.

2.2. TGA Pyrolysis experiments

Pyrolysis experiments were carried out with a novel TGA-based methodology specifically developed by Piazza et al. [25] for cellulose pyrolysis to achieve a complete characterization of the product slate. Fig. 1 displays a schematization of this methodology, extensively presented and described in [25]. Adjustments of the operating parameters were made in order to fit the procedure also for hemicellulose.

The pyrolysis experiments were conducted using a thermogravimetric analyzer (Hitachi STA7300 TG-DTA), where biomass samples (approximately 12 mg for xylan, 16 mg for glucomannan and 18 mg for arabinoxylan) were placed inside a ceramic crucible and heated up at five different controlled heating ramps (3 °C/min, 10 °C/min, 20 °C/min, 50 °C/min and 100 °C/min). The TGA chamber was continuously flushed with a high helium flow (275 Nml/min), ensuring rapid transport of volatile products out of the hot zone. This configuration was designed to minimize the residence time of vapors and thereby suppress secondary gas-phase reactions, enabling the focus to remain on the devolatilization step. Moreover, given the extremely fine hemicellulose powders ($d_P \ll 500$ micron), intraparticle secondary reactions could play a role only at the slowest heating rate (3 °C/min), but their impact is expected to be minimal due to the high dilution and low temperature. During the experiment, continuous measurements of sample weight were taken, and thermogravimetric (TG) and differential thermogravimetric (DTG) curves were generated.

The solid residual present on the crucible at the end of the experiment represents biochar, the solid carbon-rich product of biomass pyrolysis. Therefore, from the TG curve it was possible to calculate the yield of biochar, as the percentage of remaining mass at 950°C.

2.3. Online MS analysis of gases and water

Monitoring of gaseous products evolved from the pyrolysis of the different biomass samples was achieved using a quadrupole mass spectrometer (HPR-20 EGA, Hiden Analytical) with SEM (Secondary Electron Multiplier) detector. This instrument was directly connected to the TGA chamber with a quartz inert capillary line (heated at 250°C). At the TGA outlet two Orbo-609 traps (Supelco), containing a sorbent material, were placed to retain all heavy oxygenated species produced during the pyrolysis process to prevent blocking of the capillary line. In this setup gases (CO, CO_2, CH_4) and H_2O were analyzed in real-time across a wide range of heating rates, enabling the direct association of their production dynamics with TG curves. Moreover, proper calibration procedures were developed [25] to convert the qualitative information obtained into quantitative data, enabling the calculation of instantaneous gas production rates (mg/min) and, after integration, the total mass yields of each species according to Eq. 1

$$Y_i = \frac{m_i}{m_{bio,0}} * 100 \quad [\%] \tag{1}$$

where $m_{bio,0}$ and m_i represent respectively the initial mass of biomass and the total mass of the produced species. Further details on the quantitative analytical protocol are provided in Section S1 of the Supplementary Material.

Real-time monitoring of pyrolysis gaseous products is particularly important for hemicellulose, especially xylan, where gaseous products constitute a significant portion of the pyrolysis output, contributing between 30 % and 45 % of the total mass yield.

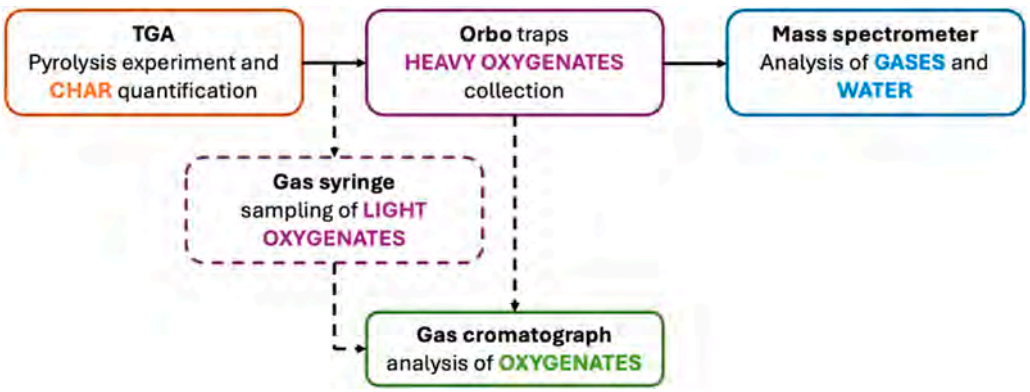

Fig. 1. TGA-based experimental setup for biomass pyrolysis analysis [25].

2.4. Offline GC analysis of bio-oil

In order to identify and quantify both light and heavy condensable products resulting from biomass pyrolysis (i.e. oxygenated compounds in the range of C_1-C_9), off-line analyses were performed with a GC equipped with FID and MS detectors (Agilent 6890, 5973 MSD) and with a HP-5MS capillary column (30 m x 250 μm x 0.25 μm). This dual-detection setup enabled comprehensive analysis, with GC-MS providing qualitative identification of compounds based on a National Institute of Standards and Technology (NIST) mass spectral library, and GC-FID allowing for quantitative measurements. The specific procedure used to obtain the quantitative speciation is reported in Section S1 of the Supplementary Material.

Two distinct sampling protocols were developed to collect respectively light and heavy condensable pyrolysis products for offline GC analysis.

Heavy products were collected using two Orbo traps (Supelco) in series, placed at the TGA outlet. After the experiments the retained products were eluted from the sorbent material with a solution containing acetone and a known amount of 1-Fluoronaphthalene, used as internal standard for the quantitative analysis in the GC-FID. The obtained liquid mixture was injected into the GC where a constant increase of the temperature from 40°C to 300°C at 10 °C/min was used. To ensure the effective trapping of condensable pyrolysis products Orbo 609 sorbing tubes, containing Amberlite® XAD®-2 (400/200 mg), were used thanks to their optimal retention capacity and compatibility with acetone for desorption. Other tested sorbents were found to be either excessively retentive, hindering desorption and quantification, or insufficient in retaining the desired compounds, leading to incomplete trapping.

Instead, pyrolysis vapors were directly sampled from the outlet of the TGA when the devolatilization rate was maximum and were immediately injected into the GC using a gas sampling syringe with 2.5 ml volume. Due to the richness of very light products (C_1-C_4) for hemicellulose pyrolysis an optimized procedure for the GC-FID analysis was developed, due to the similar retention time of the analyzed compounds. In particular, during the GC analysis, a heating ramp of 1 °C/min was used up to 150°C, where the majority of the products reach the end of the column, while a faster ramp (10 °C/min) was used up to 300°C.

Thanks to this protocol a complete mass balance closure, including the quantification of bio-oil product yields, was achieved at 100 °C/min. At this heating rate, pyrolysis generates a sharp pulse of products over a very short time, resulting in higher concentrations that can be effectively captured using gas sampling syringes and ORBO sorbent traps. An attempt was also made to achieve complete quantitative speciation of the bio-oil fraction at a lower heating rate (20 °C/min). Due to the greater dilution of pyrolysis products at this condition, the ORBO tubes placed at the outlet of the TGA were immersed in an ice bath to enhance condensation. This proved to be effective in the case of arabinoxylan, possibly thanks to the high concentration of easily condensable sugars in the bio-oil fraction. Instead, for xylan and glucomannan, the ORBO traps proved ineffective despite the lower condensation temperature. Still, bio-oil species sampled with the gas syringe could be analyzed in terms of relative GC areas, as presented in the Results section.

2.5. Lumped kinetic scheme of hemicellulose pyrolysis

To simulate biomass pyrolysis experiments, the lumped kinetic models proposed by Debiagi et al. [18] and Dussan et al. [19] were used. Their approach is to group numerous individual chemical species into a few representative categories, or "lumps," which correspond to broader chemical classes. Lumped reactions and lumped species of these models were built from the literature data on hemicellulose pyrolysis available at the time. The details of the two kinetic schemes can be found in the Supplementary material (Section S4). Simulations of the TG experiments were performed using OpenSMOKE++, an open-source software suite for modeling reactive systems, which supports various kinetic mechanisms in CHEMKIN format and can handle both gas-phase and solid-phase reactions [6]. The lumped mechanism was integrated into a zero-dimensional reactor model, with each simulation using the initial biomass mass, and temperature program as input parameters to match those of the experimental setup. Experimental data were compared with model predictions to highlight the benefits of a comprehensive dataset in refining and upgrading kinetic models. These models [18,19] are in fact semi-empirical and their accuracy mirrors the accuracy of available experimental data.

3. Results and discussion

3.1. Devolatilization behavior of hemicellulose

The pyrolytic behavior of xylan, glucomannan and arabinoxylan was investigated through TGA experiments as detailed in section 2.2.1. TG curves are calculated on a dry basis, thus eliminating the contribution of the moisture released by the biomass sample below 150°C, which accounts for approximately 10 % of the initial weight of biomass for arabinoxylan, 12 % for glucomannan and 13 % for xylan.

In Fig. 2 TG and DTG curves for the analyzed hemicelluloses at 20 °C/min are presented. The devolatilization profiles indicate that different polysaccharides exhibit distinct and characteristic pyrolysis behaviors. Overall, as evident from the TG curves, mass loss occurs within a similar temperature range for all hemicelluloses, typically falling between 200–350°C. The TG curves also reveal the multi-step nature of hemicellulose devolatilization, where changes in slope indicate distinct decomposition stages. The least thermally stable hemicellulose is xylan, undergoing decomposition at the lowest temperature, followed by glucomannan and arabinoxylan. This low thermal stability corresponds to a higher yield of solid residue that in fact decreases from xylan to glucomannan to arabinoxylan.

As reported by mechanistic studies present in the literature [8,28,37], the observed multi-faceted behavior mirrors the inherent diversity of hemicellulose polymers, both in terms of structure and chemical composition. The pentose or hexose-based backbone structure and the different lateral substituents may undergo partial or complete devolatilization at distinct stages. As represented in Table 1 the xylan tested in this work is composed of a xylose backbone chain with lateral glucuronic acid moieties, the glucomannan is a co-polymer of glucose and mannose, while the arabinoxylan has arabinose monomers linked to the main xylose chain.

The DTG curves offer a clearer depiction of the multi-step devolatilization of hemicellulose especially for xylan and arabinoxylan. In Fig. 2B xylan shows two major peaks at 265°C and at 312°C. The first peak can be ascribed to the decomposition of side-chain structure (such as the 4-O-methyglucuronic acid unit), and the second one should be attributed to fragmentation of the depolymerized units, as reported by Shen et al. [29]. For temperatures higher than 350°C, Chen et al. [8] reported that the continuous weight loss displayed by the TG curve is associated with the rearrangement of the solid residue with release of species in the gas phase and with charring process.

Glucomannan shows instead a unique devolatilization peak at 319°C, due to its more regular hexose-based structure. Similar TG and DTG trends were observed by Moriana et al. [23] testing a glucomannan extracted from spruce wood. They also reported that the devolatilization of glucomannan could exhibit a dual-stage behavior similar to that of xylan, due to the presence of two distinct monomers—mannose and glucose—in its main chain. The observed single devolatilization peak may result from the overlapping of the individual devolatilization peaks of these monomers, as both decompose within a similar temperature range.

Finally, arabinoxylan displays once again a dual peak behavior, with a main peak at 312°C and a secondary contribution at 358°C, similarly to what reported by Werner et al. [28]. The main peak, visibly

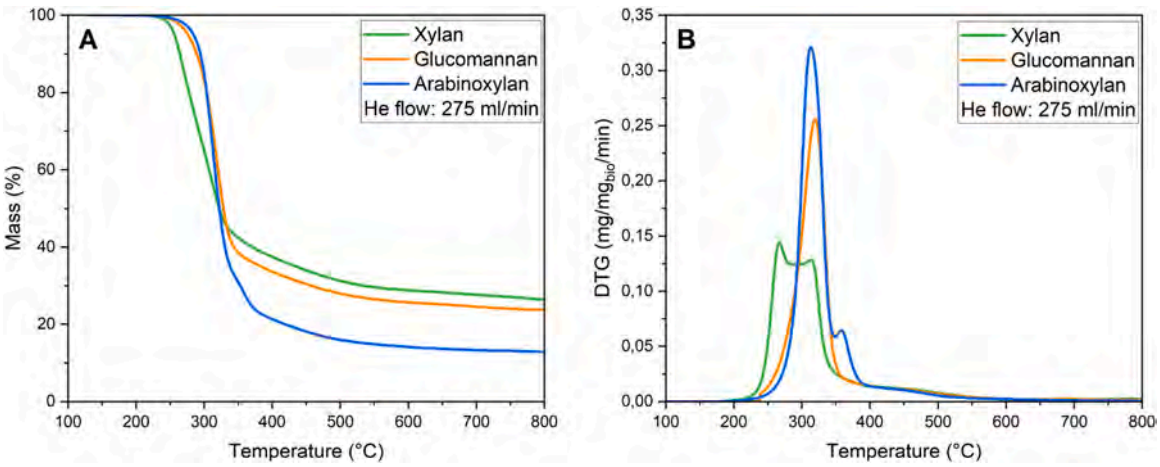

Fig. 2. TG (A) and DTG (B) curves for xylan, glucomannan and arabinoxylan at 20 °C/min.

overlapping to glucomannan main devolatilization event and to the second peak of xylan DTG is likely correlated to the onset of the chain depolymerization.

Table 2 reports elemental analyses of the solid residue for the different samples. Biochar is primarily composed of carbon, though small amounts of hydrogen and oxygen are also present. Generally, higher carbon purity is more desirable in biochar. The carbon content in biochar is influenced by various factors, including biomass type, pyrolysis temperature, residence time, ash content, and biomass moisture content [38]. Among the samples, xylan produced biochar with the highest carbon content and the lowest oxygen content, although the differences between all analyzed samples were relatively small.

For all three samples, the carbon content was found to be quite high while hydrogen content was instead quite low. Typically, hemicellulose char samples contain between 1.5–2 % hydrogen, while O/C ratio range between 0.1 and 0.2 [39,40]. However, both Smith et al. [41] and Ma et al. [42] observed that increasing the char collection temperature leads to a decrease in hydrogen content, with values dropping from about 5 % at 300°C to 1 % at 700°C as well as in an increase in the carbon content from about 40 % at 300°C to 90°C at 850°C. In this study, char samples were collected at the end of the pyrolysis experiment in the TGA, reaching a final temperature of 950°C, which is likely the reason for the high amount of carbon and the low amount of hydrogen found in the elemental analysis.

Hemicellulose samples were also tested at different heating rates. Fig. 3 displays TG and DTG curves for xylan, glucomannan and arabinoxylan at 3 °C/min, 10 °C/min, 20 °C/min, 50 °C/min and 100 °C/min. With higher heating rates, the onset of the pyrolysis process shifts to higher temperatures, as expected due to the dynamic nature of the measurement. Interestingly, the temperature interval from 5 % to 50 % mass loss is similar across all heating rates, amounting to ~110 °C for xylan, ~90 °C for glucomannan, and ~70 °C for arabinoxylan, in agreement with studies conducted under similar condition [10,29].

In the case of glucomannan and xylan, a higher heating rate correlates with a lower production of biochar. For xylan the biochar yield at 100 °C/min is 23 % while at 3 °C/min is 25 %. For glucomannan the biochar yield at 100 °C/min is 19 % while at 3 °C/min is 25 %. Conversely, arabinoxylan exhibits a constant production of solid residue (around 13 %) with a negligible difference in mass yield.

The DTG curves (Fig. 3 B-D-F) show that by increasing the heating rate, the peaks shift to higher temperatures for all tested hemicelluloses. The shift in peak temperatures (ΔT between peak DTG at 3 °C/min and 100 °C/min) is ~53°C for xylan, ~51°C for glucomannan and ~63°C for arabinoxylan. Additionally, for both xylan and arabinoxylan, higher heating rates result in the merging of distinct devolatilization contributions into a single, broader peak, consistent with findings from literature studies conducted under similar conditions. [28]

Table 2
Elemental composition of biochar from xylan, glucomannan and arabinoxylan.

	C [wt%]	H [wt%]	O [wt%]
Xylan biochar	82.90 ± 0.05	0.35 ± 0.05	16.75 ± 0.09
Glucomannan biochar	79.90 ± 0.05	0.34 ± 0.05	19.13 ± 0.09
Arabinoxylan biochar	77.81 ± 0.05	0.33 ± 0.05	20.19 ± 0.09

3.2. *Speciation of hemicellulose pyrolysis products*

The objective of this work is to assess a characteristic product slate for each model biomass, both qualitatively and quantitatively, to highlight unique features and behaviors and to analyze the effect of the heating rate. This study builds upon previous work by some of the authors [26], which provided an initial assessment of product speciation for xylan and glucomannan. Expanding on that foundation, this work introduces new insights, including online measurements of gaseous products during hemicellulose pyrolysis at different heating rates, detailed bio-oil speciation across heating rates, and the extension of the analysis to arabinoxylan. Together, these advancements offer a comprehensive view of hemicellulose pyrolysis. The extensive dataset collected in this study is unparalleled in existing literature and provides deep insights into the governing stoichiometries with invaluable benefit for the advancement and validation of kinetic models.

First the online analysis of gaseous products and H_2O will be presented, together with their integral yields for various heating rates. Then the detailed speciation of the bio-oil fraction obtained at 100 °C/min will be shown. Finally, the distribution of the products among solid, liquid and gaseous fraction will be reported for various heating rates.

3.2.1. *Online analysis of gases and H_2O*

The monitoring of the dynamic evolution of gaseous products, such as CO, CO_2 and CH_4, throughout the pyrolysis process is crucial to link their production to specific thermal events as well as tune decomposition kinetics. In fact, these products constitute a significant portion of hemicellulose pyrolysis products, as also highlighted in previous studies [8,10,26,28,34,43],

Fig. 4 illustrates the online monitoring of gaseous species (CO, CO_2, H_2O and CH_4) together with the sum of their signals (left panels), compared to the DTG curves (right panels) at 20 °C/min. In each case, the production patterns of these species closely mirrored the dynamics of hemicellulose devolatilization, described by the DTG curves.

Below 450°C, for all three hemicelluloses a substantial release of CO, CO_2 and H_2O accompanied the main devolatilization event. The lower

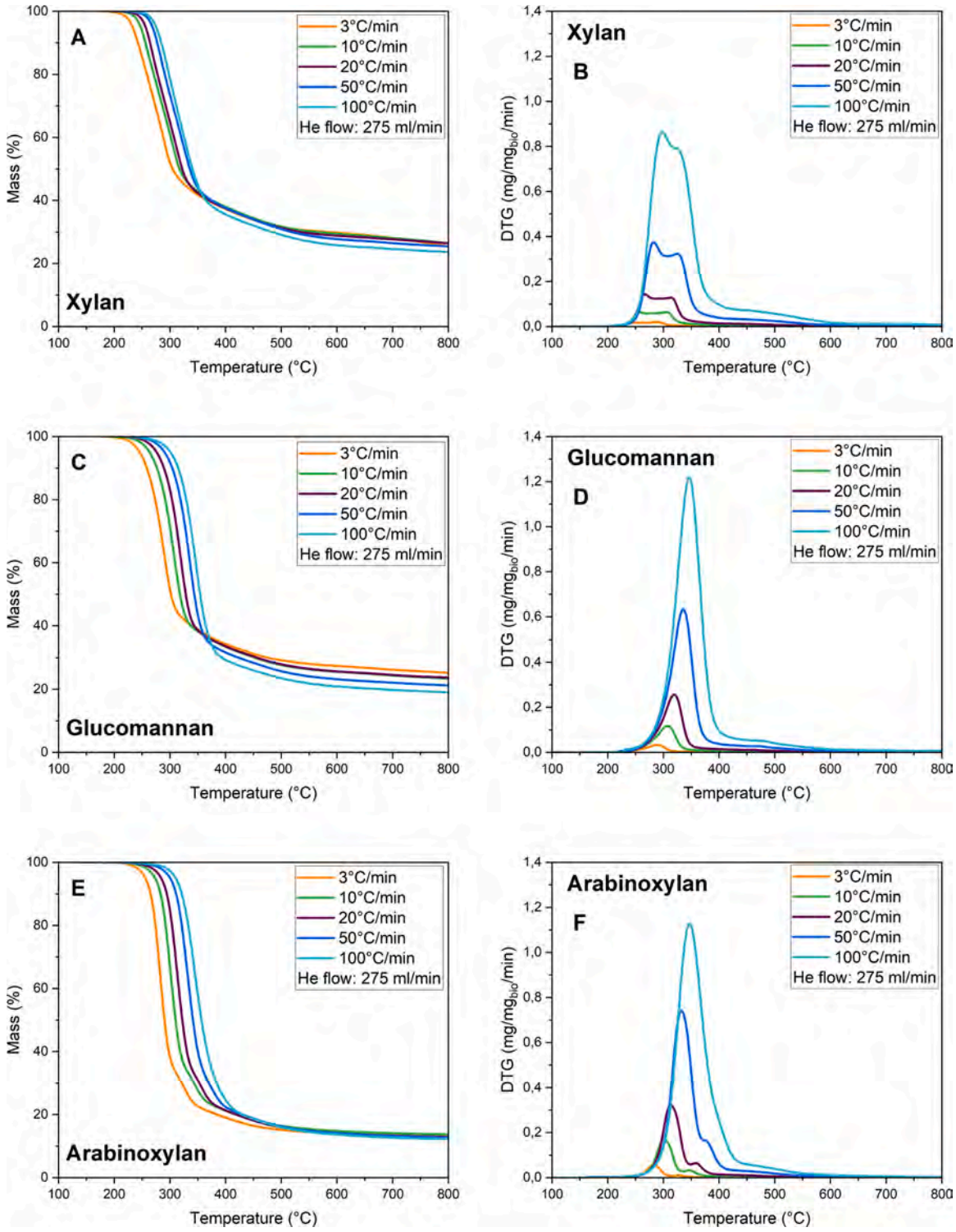

Fig. 3. TG (A,C,E) and DTG (B,D,F) curves for xylan, glucomannan and arabinoxylan at 3 °C/min, 10 °C/min, 20 °C/min, 50 °C/min and 100 °C/min.

intensity of the total gas production profile with respect to that of DTG reveals the formation of condensable C_2–C_{6+} volatiles, which will be analyzed in Section 3.2.2. On a qualitative basis, it is observed that the shape of the gas trends replicates that of the DTG curves. Xylan displays broad gas production peaks, suggesting a devolatilization behavior characterized by overlapping stages, closely following the dual-peaks profile observed in its DTG curve. Glucomannan exhibits a sharper production peak, suggesting a single devolatilization event, aligned with its DTG curve. Arabinoxylan also displays a single gas release profile, in line with the dominant devolatilization event in the DTG; the minor DTG peak at 350°C is not detected in the gas profiles, likely due to resolution limits.

At temperatures between 450°C and 600°C, the pyrolysis of all the hemicellulose was solely characterized by gas release (CH_4, CO and CO_2), without additional volatile formation. Debiagi et al. [18] explained this behavior due to a release in the gas phase of intermediates ('metaplastic species') retained within the solid matrix of the decomposing biomass. Both in the DTG curves and the gas release profile of all

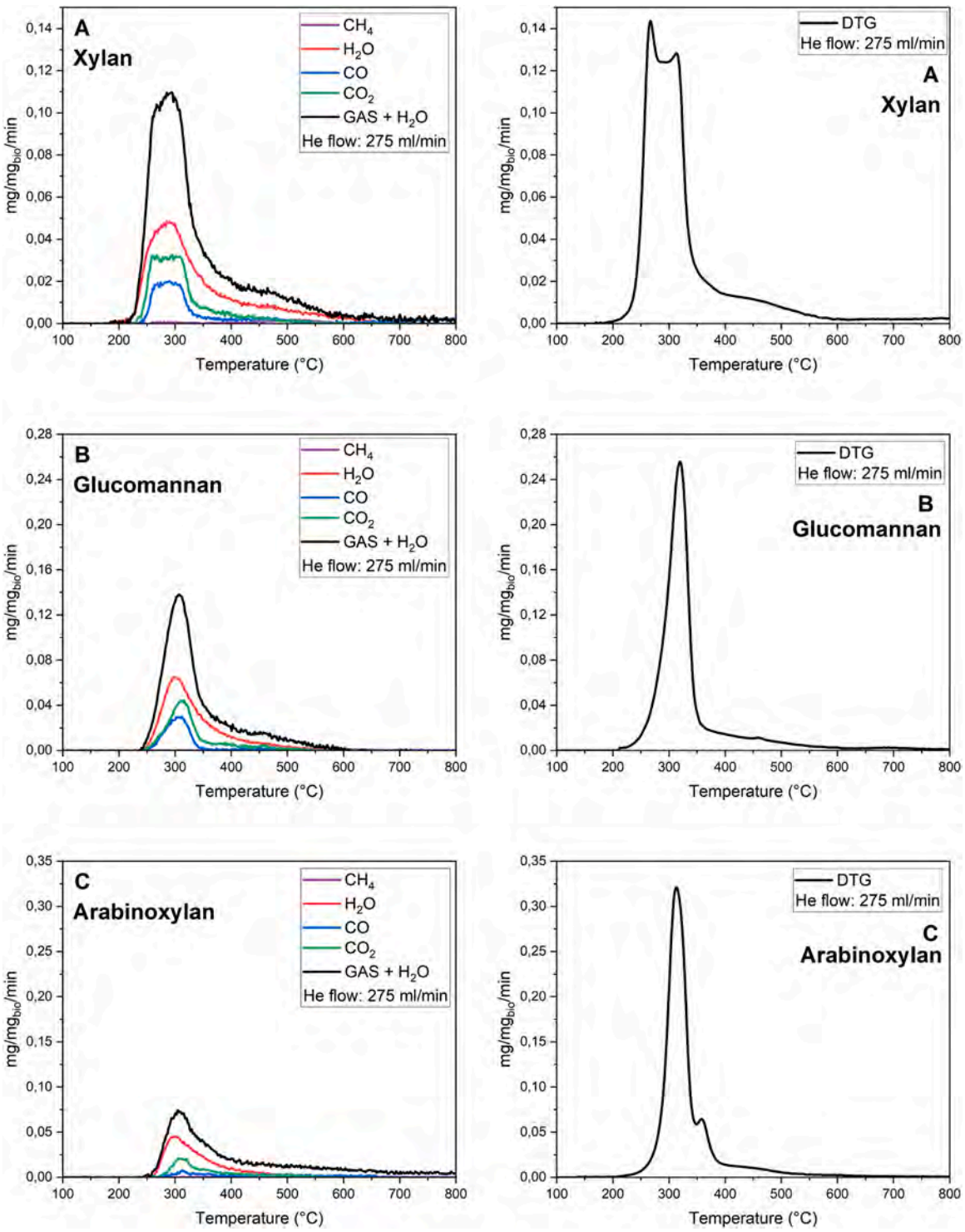

Fig. 4. Online monitoring of gases (CO, CO_2, CH_4) and H_2O (left panels) and DTG curves (right panels) during xylan, glucomannan and arabinoxylan pyrolysis at 20 °C/min.

three hemicelluloses this second stage corresponds to the spreading of the main peak between 450°C and 600°C.

Finally, at higher temperatures (>600°C), a minor impact of charring reactions is observed, characterized by the aromatization, condensation, and cross-linking of the remaining solid matrix, leading to the formation of a carbon-rich char and the concomitant release of minor amounts of gases such as CO, CO_2, and CH_4. These reactions are consistent with those reported in the literature [18,19,44], describing the thermal degradation and carbonization of hemicellulose residues.

Among the hemicelluloses studied, xylan exhibits the highest yield of gaseous products, arabinoxylan the lowest, and glucomannan an intermediate yield; it is observed that DTG curves resemble the summation of flowrates curves when the yields of these species become more significant.

The complete dataset for the online monitoring of water and gas production is provided in the Supplementary Material (S2), including dynamic profiles alongside DTG curves for all investigated heating rates (3 °C/min, 10 °C/min, 50 °C/min, and 100 °C/min). It is important to

underline that at heating rates of 50 °C/min and 100 °C/min, the online monitoring of H_2O becomes challenging due to the short experiment duration, and H_2O tendency to condense on the connection lines and ORBO, before a gradual release. To indicate the uncertainty of the online signal, the H_2O flowrate at these rates is plotted as a dashed line.

The real-time quantification of gases and H_2O also allowed for the calculation of species yields (Eq. 1) using the protocol described in Section S1.1 of the Supplementary Material. Fig. 5 presents the calculated integral mass yields for these species for xylan, glucomannan, and arabinoxylan across all heating rates studied. All measurements are accompanied by their respective experimental errors, which are also shown in Fig. 5, calculated based on 3 replicates of the same experiment.

The measurement uncertainty is ±1 % for methane, ±3 % for CO, and ±4 % for CO_2. Water exhibits a higher uncertainty (±6 %) due to the complexity of the calibration procedure required to determine its response factor, detailed in [25], as well as its challenging behavior during the experiment.

Some trends are identified: for xylan, the water yield increases with higher heating rates, rising from 27 % at 3 °C/min to 34 % at 100 °C/min. In contrast, the yields of CO and CO_2 decrease as the heating rate increases. For glucomannan, the water yield decreases as heating rates increase. The trends for CO and CO_2 differ and while the CO_2 yield decreases with higher heating rates, CO remains relatively stable, oscillating around 5 % across all heating rates. For arabinoxylan, the water yield exhibits a significant decline, dropping from 46 % at 3 °C/min to 20 % at 100 °C/min. Unlike the other hemicelluloses, no clear trends are observed for either CO or CO_2. Noteworthy, the CO:CO_2 ratio (0.4 for xylan and glucomannan and 0.6 for arabinoxylan) remains fairly constant across the range of heating rates analyzed.

Moreover, for all three hemicelluloses, CH_4 is a minor product, negligible at higher heating rates and appreciable only at the slowest rate (≈5 wt% at 3 °C/min). Its formation can be associated with secondary cracking reactions, which are more pronounced at lower heating rates. CH_4 can therefore serve as a marker of the extent of secondary reactions in our setup, which remain, however, very limited.

3.2.2. *Speciation of bio-oil*

Quantitative speciation of the liquid organic fraction was achieved for all hemicelluloses at the fastest heating rate (100 °C/min). This condition facilitated rapid decomposition kinetics and produced a sharp pulse of volatiles, enabling efficient collection of the products in the Orbo trap.

Table 3 presents the integral mass yields of each identified species for xylan, glucomannan, and arabinoxylan pyrolysis, along with the elemental composition of the product pool for each hemicellulose. The data refine and extend the work previously conducted by some of the authors [26], offering a more comprehensive characterization of liquid-phase products from hemicellulose pyrolysis. The bio-oil obtained from hemicellulose pyrolysis exhibited a diverse product distribution, including ketones, aldehydes, furanic species, anhydrosugars, monosaccharides, other cyclic oxygenates, and aromatic compounds with carbon chain lengths ranging from C_1 to C_{6+}.

In all three cases, no single compound emerged as dominant product in the bio-oil fraction. Instead, a wide array of species was identified, each contributing in little amount to the total mass yield. Specifically, 29, 41, and 26 condensable oxygenates were identified and quantified for xylan, glucomannan, and arabinoxylan pyrolysis, respectively.

For clarity, Fig. 6 illustrates the bio-oil composition in terms of total mass yield, grouping products by chemical functionality and categorizing them by carbon chain length. In the case of xylan (Fig. 6 A), at 100 °C/min aliphatic ketones represented the predominant class of condensable products, followed by furanic species, esters and cyclic oxygenates. These products were distributed across the C_1–C_9 range. Notably, no anhydrosugars were detected, and specifically, the C_5 anhydrosugar associated with xylan depolymerization, anhydro-xylose, was absent. This behavior appears to be linked to structural features of

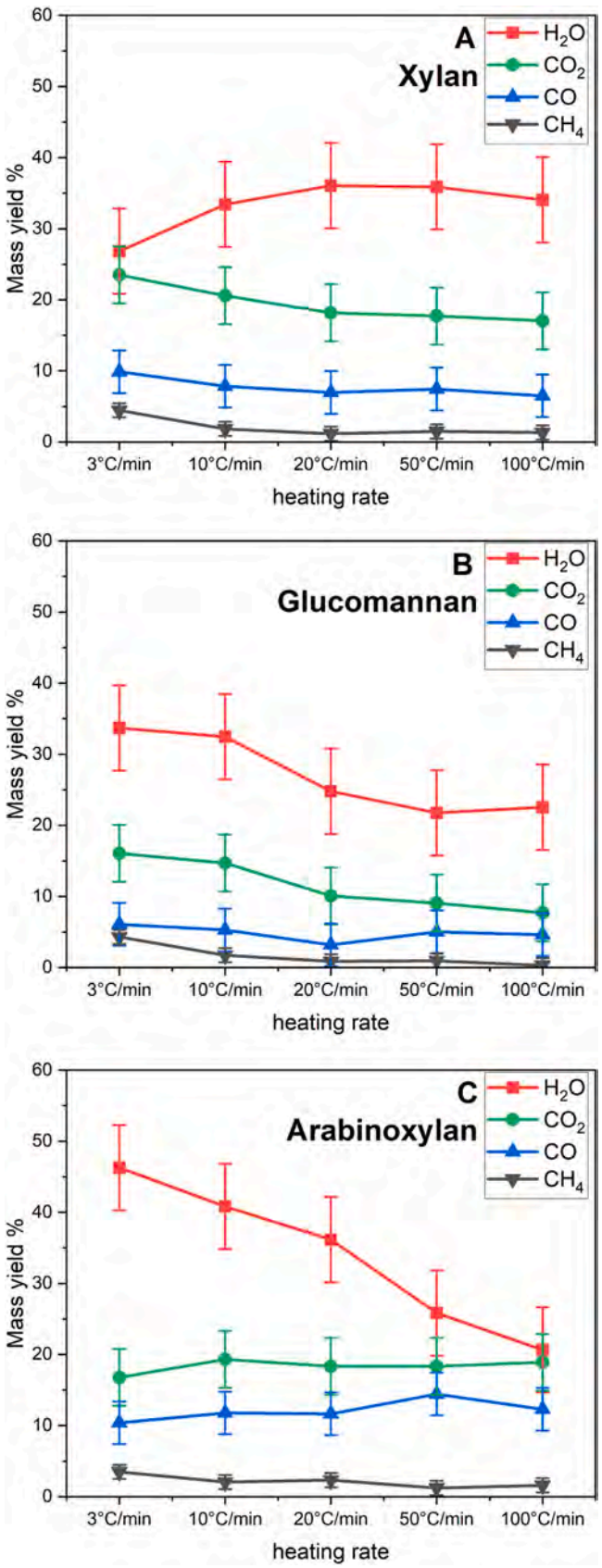

Fig. 5. Integral mass yields of single gaseous species for xylan, glucomannan and arabinoxylan.

Table 3
Quantitative speciation of bio-oil organic species for xylan glucomannan and arabinoxylan pyrolysis at 100 °C/min.

ketones and aldehydes [mass yields %]				
		xylan	**glucomannan**	**arabinoxylan**
formaldehyde	CH_2O	0.1	< 0.1	< 0.1
acetaldehyde	C_2H_4O	2.3	< 0.1	< 0.1
methyl glioxal	$C_3H_4O_2$	-	-	< 0.1
acetone	C_3H_6O	0.3	0.1	0.3
2-propanone, 1-hydroxy	$C_3H_6O_2$	-	0.7	-
2,3 butanedione	$C_4H_6O_2$	0.7	0.3	0.1
succindialdehyde	$C_4H_6O_2$	-	0.4	-
hydroxyacetaldehyde	$C_2H_4O_2$	-	0.1	-
acetic anhydride	$C_4H_6O_3$	-	-	0.1
2-butanone	C_4H_8O	0.4	-	-
2,3 pentanedione	$C_5H_8O_2$	0.4	0.5	0.2
glutaraldehyde	$C_5H_8O_2$	-	0.7	-
2-furancarboxaldehyde, 5-methyl	$C_6H_6O_2$	-	0.5	-
acids and alcohols [mass yields %]				
		xylan	**glucomannan**	**arabinoxylan**
acetic acid	$C_2H_4O_2$	-	0.3	-
propanoic acid, 2-oxo-, methyl ester	$C_4H_6O_3$	-	0.5	-
1-ethylcyclopropanol	$C_5H_{10}O$	-	-	0.2
propanoic acid, 2,2-dimethyl-	$C_5H_{10}O_2$	0.7	-	-
furan derivatives [mass yields %]				
		xylan	**glucomannan**	**arabinoxylan**
furan	C_4H_4O	0.1	< 0.1	-
2,3-*dihydrofuran*	$C_4H_6O_3$	-	-	< 0.1
furan, 2,5-*dihydro*	C_4H_6O	-	-	0.3
2(5 H)-furanone	$C_4H_4O_2$	-	0.5	-
2(3 H)-furanone, dihydro−4-hydroxy-	$C_4H_6O_3$	-	0.4	-
2-furanol, tetrahydro−2-methyl-	$C_5H_{10}O_2$	-	0.2	-
furan, 2-methyl-	C_5H_6O	0.1	0.4	0.1
2-furanmethanol	$C_5H_6O_2$	-	3.5	-
2(3 H)-furanone, 5-methyl-	$C_5H_6O_2$	0.1	-	-
2-furanmethanol, tetrahydro-	$C_5H_{10}O_2$	-	1.4	-
furfural	$C_5H_4O_2$	0.1	0.4	2.0
2,4(3 H,5 H)-furandione,3-methyl	$C_5H_6O_3$	-	-	0.2
furan, 2,5-dimethyl	C_6H_8O	-	0.2	-
2,5-dimethyl−4-hydroxy−3(2 H)-furanone	$C_6H_8O_3$	-	0.9	-
ethanone, 1-(2-furanyl)-	$C_6H_6O_2$	-	1.7	0.3
5-hydroxymethylfurfural	$C_6H_6O_3$	-	3.0	-
5-acetoxymethyl−2-furaldehyde	$C_8H_8O_4$	-	1.8	-
furan, 2-(2-propenyl)-	C_7H_8O	0.1	-	-
cyclo oxygenates [mass yields %]				
		xylan	**glucomannan**	**arabinoxylan**
butyrolactone	$C_4H_6O_2$	-	0.4	0.2
2-hydroxy-gamma-butyrolactone	$C_4H_6O_3$	0.3	1.0	-
cyclo propyl carbinol	C_4H_8O	0.4	1.3	-
1,2-cyclopentanedione	$C_5H_6O_2$	-	1.5	-
cyclopentanol	$C_5H_{10}O$	0.3	1.1	-
1,2-cyclopentanediol, trans-	$C_5H_{10}O_2$	-	0.6	-
1,2-cyclopentanedione, 3-methyl-	$C_6H_8O_2$	0.3	0.9	-
2-cyclohexen−1-ol	$C_6H_{10}O$	-	0.8	-
1,4-dioxaspiro(2,4)heptan−5-one, 7-methyl	$C_6H_8O_3$	-	0.7	-
3-hexanone	$C_6H_{12}O$	0.2	-	-
3,4-hexanedione	$C_6H_{10}O_2$	0.1	-	-
1,3-dioxane−4,6-dione, 2,2-dimethyl-	$C_6H_8O_4$	-	-	0.6
2-cyclopenten−1-one, 3-ethyl−2-hydroxy-	$C_7H_{10}O_2$	-	0.8	-
2-cyclopenten−1-one, 3,4-dimethyl-	$C_7H_{10}O_2$	0.1	-	-
4,4-dimethyl−2-cyclopenten−1-one	$C_7H_{10}O$	0.1	-	-
1,2-dioxolan−3-one, 5,5-diethyl−4-methylene-	$C_8H_{12}O_3$	1.4	-	-
ethers and esters [mass yields %]				
		xylan	**glucomannan**	**arabinoxylan**
ethyl−1-propenyl ether	$C_5H_{10}O$	0.3	-	0.2
sugars [mass yields %]				
		xylan	**glucomannan**	**arabinoxylan**
dianhydroxylose - I	$C_5H_6O_3$	-	-	7.6
dianhydroxylose - II	$C_5H_6O_3$	-	-	1.6
1,4-anhydro-D-xylopyranose - I	$C_5H_8O_4$	-	-	4.5
1,4-anhydro-D-xylopyranose - II	$C_5H_8O_4$	-	-	4.0
DL-arabinose	$C_5H_{10}O_5$	-	-	0.9
levoglucosenone	$C_6H_6O_3$	-	0.6	-
1,4:3,6-dianhydro-α-D-glucopyranose	$C_6H_8O_4$	-	1.7	0.1

(*continued on next page*)

Table 3 (*continued*)

2,3-anhydro-D-mannosan	$C_6H_{10}O_5$	-	1.0	-
beta-D-glucopyranose, 1,6-anhydro	$C_6H_{10}O_5$	-	9.8	1.7
D-allose	$C_6H_{12}O_6$	-	4.6	1.1
aromatics [mass yields %]				
		xylan	**glucomannan**	**arabinoxylan**
catechol	$C_6H_6O_2$	0.4	0.6	-
benzyl alcohol	C_7H_8O	0.1	-	-
2,3-dihydroxybenzaldehyde	$C_7H_6O_3$	0.9	-	-
1,2-benzenediol, 3-methyl-	$C_7H_8O_2$	0.9	-	-
phenol, 2,5-dimethyl-	$C_8H_{10}O$	0.2	-	-
resorcinol, 2-acetyl-	$C_8H_8O_3$	0.4	-	-
benzopyran	C_9H_8O	1.0	-	-
elemental composition [wt%]				
		xylan bio-oil	**glucomannan bio-oil**	**arabinoxylan bio-oil**
C		63.1	53.0	51.0
H		7.9	6.8	5.4
O		29.0	40.2	43.6

the xylan polymer, which markedly distinguish it from its monomer (xylose) and its dimer (xylobiose). In this respect, Hu et al. [45] investigated the pyrolysis of xylan, xylose and xylobiose, reporting that anhydrosugar formation decreased from monomer to dimer and was almost completely absent for xylan. He reported that the higher DP value of the polymer, compared to the monomer and the dimer, inhibits depolymerization and cracking reactions during xylan fast pyrolysis resulting in the absence of anhydrosugars, relatively low yields of volatile organic products (which in this study were found limited to 12.9 %), and a preference for gaseous species. Moreover, other studies by Wang et al. [31] and Shen et al. [29] reported that the branched structure of xylan favors the formation of gaseous products over bio-oil, particularly heavier compounds such as sugars. It is also noteworthy that the presence of aromatic compounds shown in Fig. 6 A likely indicates contamination of the xylan powder with lignin-derived structures, potentially originating from the extraction process. Additionally, acetic acid was not detected in this study, which is surprising given that it is typically produced from the cleavage of 2-O-acetyl xylopyranose [11, 31]. The absence of acetic acid may suggest a lack of acetyl side groups in the commercial xylan used. At 20 °C/min the distribution of the main product categories was largely consistent with the distribution seen at 100 °C/min, with only a slightly higher presence of ketones and esters at the slower ramp, alongside the absence of aromatic impurities and aliphatic acids. More information can be found in the supplementary material (Section S3).

In contrast to xylan, both glucomannan and arabinoxylan produced larger amounts of organic bio-oil (42,9 % and 26,6 % respectively). For glucomannan, anhydrosugars and furanic compounds were the most prominent fractions, followed by other cyclic oxygenates. Unlike xylan, glucomannan showed a significant monomeric unit release, as evidenced by the substantial production of C_6 anhydrosugars, which accounted for 17.7 % of the total mass yield. Among these, levoglucosan was the most abundant product, followed by D-allose and 1,4:3,6-dianhydro-α-D-glucopyranose. Other notable products from glucomannan pyrolysis included hydroxymethylfurfural, furfuryl alcohol, and cyclopentanol. This product distribution aligns with previous thermal degradation studies [23,33]. However, no detailed mechanistic explanation for glucomannan's pyrolysis behavior is currently available. Moriana et al. [23] suggested that, like xylan, glucomannan pyrolysis might occur in two stages: cleavage of glycosidic bonds followed by monomer decomposition. Yet, the preference for depolymerization as the dominant decomposition pathway in glucomannan, in contrast to xylan, remains unexplained. This behavior could potentially be attributed to the absence of lateral substituents, the more regular polymeric structure of glucomannan, and the greater stability of C_6 sugars compared to C_5 sugars. Once again, a speciation was obtained also for a slower heating rate (20 °C/min) and compared to the quantitative data from the 100 °C/min experiment (Supplementary material, Section S3). The distribution of the main product categories was almost perfectly reproduced between the two heating rates, with only slightly higher production of cyclic oxygenates and lower amount of furanic species.

Finally, the analysis of arabinoxylan revealed that the majority of bio-oil products were sugars, accounting for approximately 20 % of the total mass yield. Notably, two anhydrosugars, dianhydroxylose and 1,4-anhydro-D-xylopyranose, were identified as the predominant compounds. These compounds are not included in the NIST libraries typically used for species identification but were identified based on studies by Hu et al. [45] and Duan et al. [46] which investigated the pyrolytic behavior of xylose and arabinose, the two monomeric units of the arabinoxylan polymer. Interestingly, arabinoxylan showed a significant formation of anhydrosugars, unlike xylan, regardless the similar chemical structure of the pentose monomers. This phenomenon is within the scope of network depolymerization models [17,30], but to the best of the author knowledge these models have not yet been applied to interpret this specific behavior. Other significant bio-oil products included ketones, aldehydes, furfural, and various other furan derivatives. Overall, the majority of the products contained five carbon atoms. In this case it was possible to obtain a quantitative speciation in terms of mass yield also at a slower heating rate (20 °C/min), possibly due to a higher production of easily condensable anhydrosugars with respect to the other hemicelluloses. At 20 °C/min a similar product distribution was observed, with sugars remaining the dominant product class, followed by ketones and furan derivatives. The carbon atom distribution also remained consistent under these conditions.

These key findings not only underscore the robustness of the analytical procedure employed for product speciation but also enriches the dataset, making it of great value for the development of kinetic models.

3.2.3. *Distribution among solid, liquid and gaseous products*

To summarize the data obtained for product speciation Fig. 7 shows the yields of the main product streams—gases, water, bio-oil (including all organic condensable species), and biochar—at 100 °C/min, together with the error calculated for water (±6 %), gases (±5 %) and char (±1 %). As discussed in the previous section for this heating rate, all fractions were analytically measured, achieving excellent mass balances, with total mass yields of 95.4 %, 97.0 %, and 94.5 % for xylan, glucomannan, and arabinoxylan, respectively. In addition, the closure of the elemental balances (C = 95 % ± 12 %, H = 76 % ± 9 %, O = 108 % ± 15 %) has been calculated. As discussed in Section 3.1 the closure of the hydrogen balance is less accurate due to the high temperature at which chars were obtained (950 °C) and the uncontrolled cooling phase

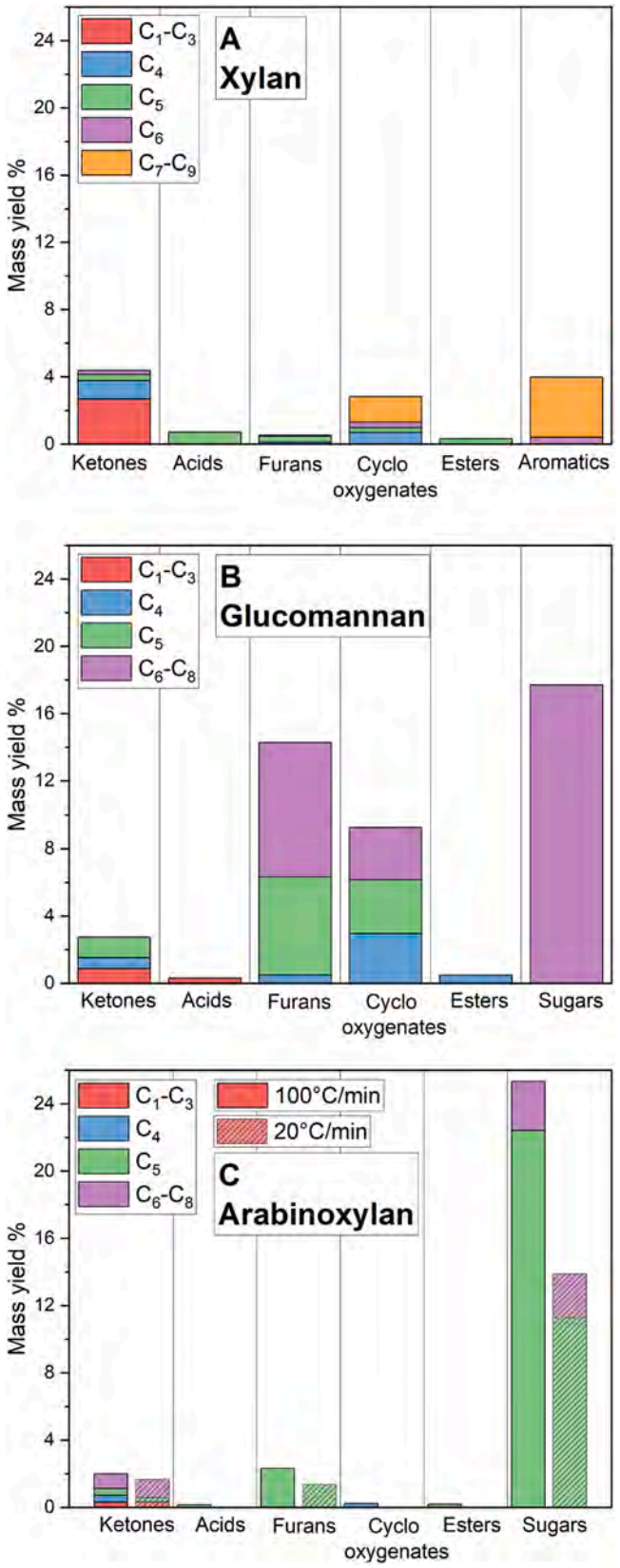

Fig. 6. Product distribution in bio-oil of xylan (A), glucomannan (B) pyrolysis at 100 °C/min, and for arabinoxylan (C) pyrolysis at 100 °C/min and 20 °C/min.

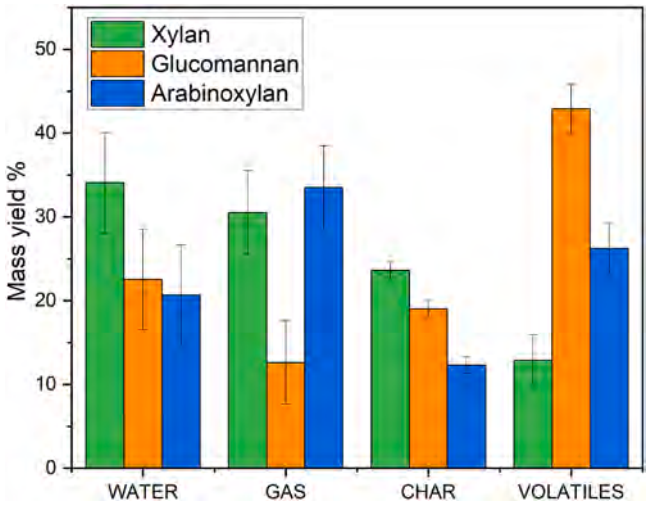

Fig. 7. Integral mass yields of xylan, glucomannan and arabinoxylan pyrolysis products at 100 °C/min.

in the TGA, during which further release of light gases and structural changes may occur. Nevertheless, the reported values remain meaningful and consistent with the elemental composition of the starting hemicelluloses (Table 1).

Xylan exhibited high yields of gases, water, and solid residue, with a relatively lower organic liquid fraction compared to the other hemicelluloses. In contrast, glucomannan showed greater production of condensable organic species, accompanied by substantial char production and reduced gas and water yields if compared to xylan. Finally, arabinoxylan displayed intermediate behavior, with products evenly distributed in all categories.

Fig. 8 shows the integral mass yields of the main product streams for xylan, glucomannan and arabinoxylan at varying heating rates, in the 3–100 °C/min range. The bio-oil yield was independently quantified for all pyrolysis tests at 100 °C/min and for arabinoxylan pyrolysis at 20 °C/min, while it is calculated as the complementary fraction to achieve full mass balance closure in the other cases.

Distinct trends in product distribution with varying heating rates for the different hemicelluloses can be observed. For xylan, water yield increased up to 20 °C/min and stayed almost constant at higher heating rates while gases decreased with the increase of heating rate, as also identified through the online monitoring of these species (Fig. 5). The biochar yield remained almost constant, while the expected yield of volatiles progressively increased. For glucomannan, the yield of water decreased with increasing heating rates. The yield of gases also showed a declining trend, consistent with the observed reduction in CO_2 and CH_4 and production at higher heating rates. Meanwhile, the biochar yield and the expected yield of volatiles followed patterns similar to those observed for xylan. For arabinoxylan, the yield of water also decreased with increasing heating rates, but the yield for gases remained fairly constant, showing no distinct pattern. The biochar yield remained relatively stable across the heating rates, while the overall yield of volatiles increased, similar to the behavior observed for the other hemicelluloses. A consistent trend was observed for organic volatiles, whose yield increased with heating rate for all the hemicelluloses, doubling in the case of xylan and tripling in the case of glucomannan and arabinoxylan.

Overall, the data highlight that a significant portion of hemicellulose pyrolysis products in all heating rates consists of gases and water. This finding underscores the importance of monitoring the online evolution of these products, reported in Section 3.2.1, to better understand the distinct steps and mechanisms involved in hemicellulose pyrolysis, as well as evaluating the potential of this stream as a fuel gas, providing insights into its composition and energy content.

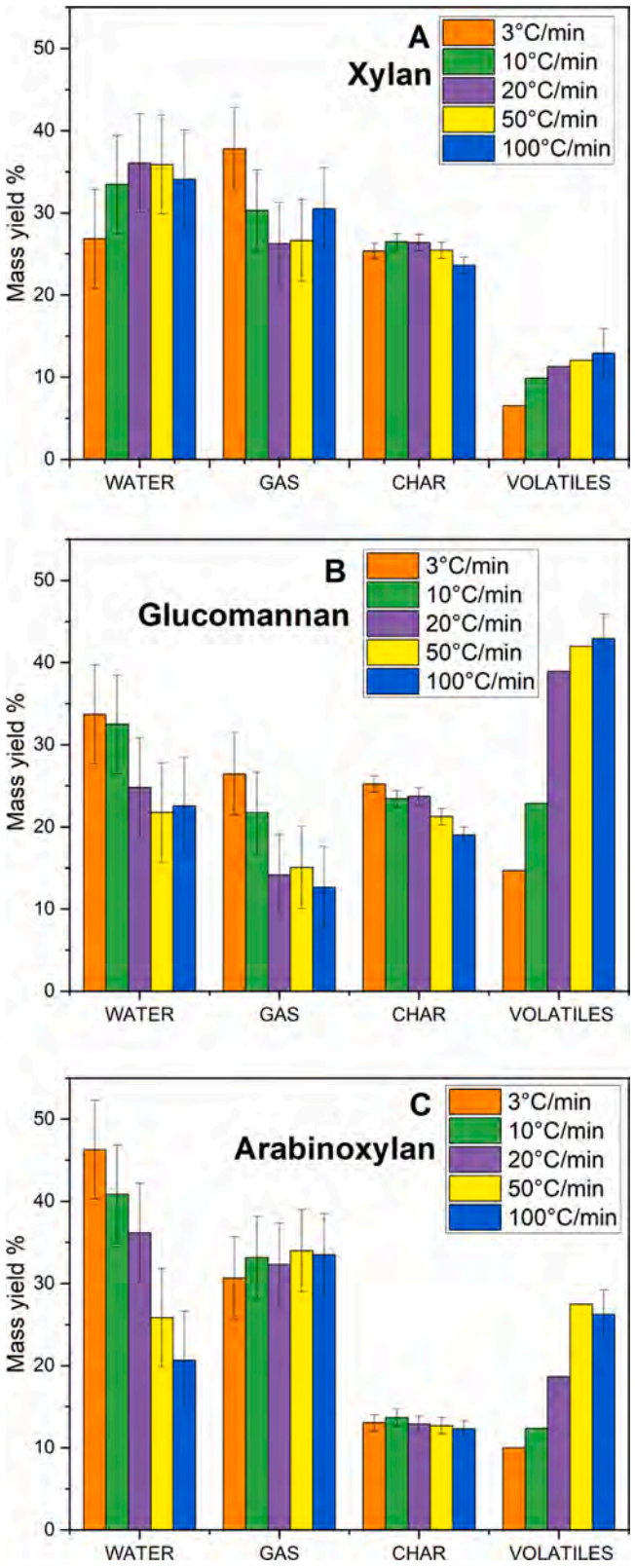

Fig. 8. Integral mass yields of xylan, glucomannan and arabinoxylan pyrolysis products at 3 °C/min, 10 °C/min, 20 °C/min, 50 °C/min and 100 °C/min.

3.3. Comparison with model predictions

The comprehensive dataset collected in this study serves as a valuable reference for the development of kinetic models. Data on devolatilization provides insights into activation energies and kinetic constants, while product speciation data forms the basis for defining the mechanism of the pyrolysis process. Furthermore, this study underscores the distinct pyrolytic behaviors of individual hemicellulosic constituents, emphasizing the importance of fundamental investigations using model biomasses before transitioning to the complexity of real biomass systems.

To illustrate the novelty and completeness of the xylan/glucomannan/arabinoxylan dataset herein reported, we extend the analysis of our previous study [26] (limited to xylan and glucomannan and with speciation at one heating rate) and compare the bulk of experimental findings with the predictions of the kinetic models by Debiagi et al. [18] and Dussan et al. [19] that are taken as descriptors of the previous state of the art on hemicellulose pyrolysis. Most of the comparisons are reported in the Supplementary Material (sections S.5-S.6) for consultation.

3.3.1. Comparison of TG curves

Fig. 9 and Figures S5.1-S5.4 show the model predictions of TG and DTG curves for xylan, glucomannan, and arabinoxylan at 3/10/20/50/100 °C/min, alongside experimental measurements.

For the TG curves, there is generally good agreement between the model predictions and the experimental data across all three hemicellulosic constituents. In particular, the sharp mass loss stage occurring between 200°C and 350°C is accurately captured. However, at higher temperatures, the predicted TG curves show additional mass loss stages that are not detected in the experimental data. These deviations also result in lower char yields in the models compared to the experimental observations.

The differences between model predictions and experimental results become more apparent when examining the DTG curves. While the primary devolatilization event is reasonably well-predicted, with the models effectively distinguishing the dual-stage or single-stage pathway of xylan, glucomannan and arabinoxylan, discrepancies emerge at higher temperatures. Specifically, the models predict additional events of volatile release, that are not observed experimentally, due to the lumping approach and to the release of gaseous species that remain in the solid phase up to higher temperatures in the so called charrification reactions.

These discrepancies are more pronounced in the model by Debiagi et al. [18], which significantly overestimates the mass loss. In contrast, the model by Dussan et al. [19] provides a closer match to the devolatilization behavior of the different biomasses, particularly in terms of the overall mass loss trends.

3.3.2. Comparison of product speciation

The value of the dataset collected in this study lies in the detailed speciation of pyrolysis products. Fig. 10 and Figure S6.1–4 compare the yields of product streams predicted by the models with experiments at 3/10/20/50/100 °C/min. As expected, significant discrepancies between the model and the data obtained in this work highlight the lack of consolidated knowledge regarding the kinetics of hemicellulose pyrolysis.

The model by Dussan et al. [19] accurately captures the distribution of products from xylan (Fig. 10 A) across the different streams. In contrast, the model by Debiagi et al. [18] significantly overestimates the yield of liquid organic products while underestimating the production of H_2O.

In the case of glucomannan (Fig. 10 B), both models overestimate the yield of gaseous products. Moreover, the model by Debiagi et al. [18] underestimates the yield for H_2O and char, while both models give a fair representation of bio-oil yield. For arabinoxylan (Fig. 10 C), both models underestimate H_2O production, the model by Debiagi [18] overestimates the yield of gaseous species, while the model by Dussan [19] underestimates char and overestimates volatiles. Overall, the discrepancies between model predictions and experimental measurements become more pronounced at lower heating rates, particularly for bio-oil

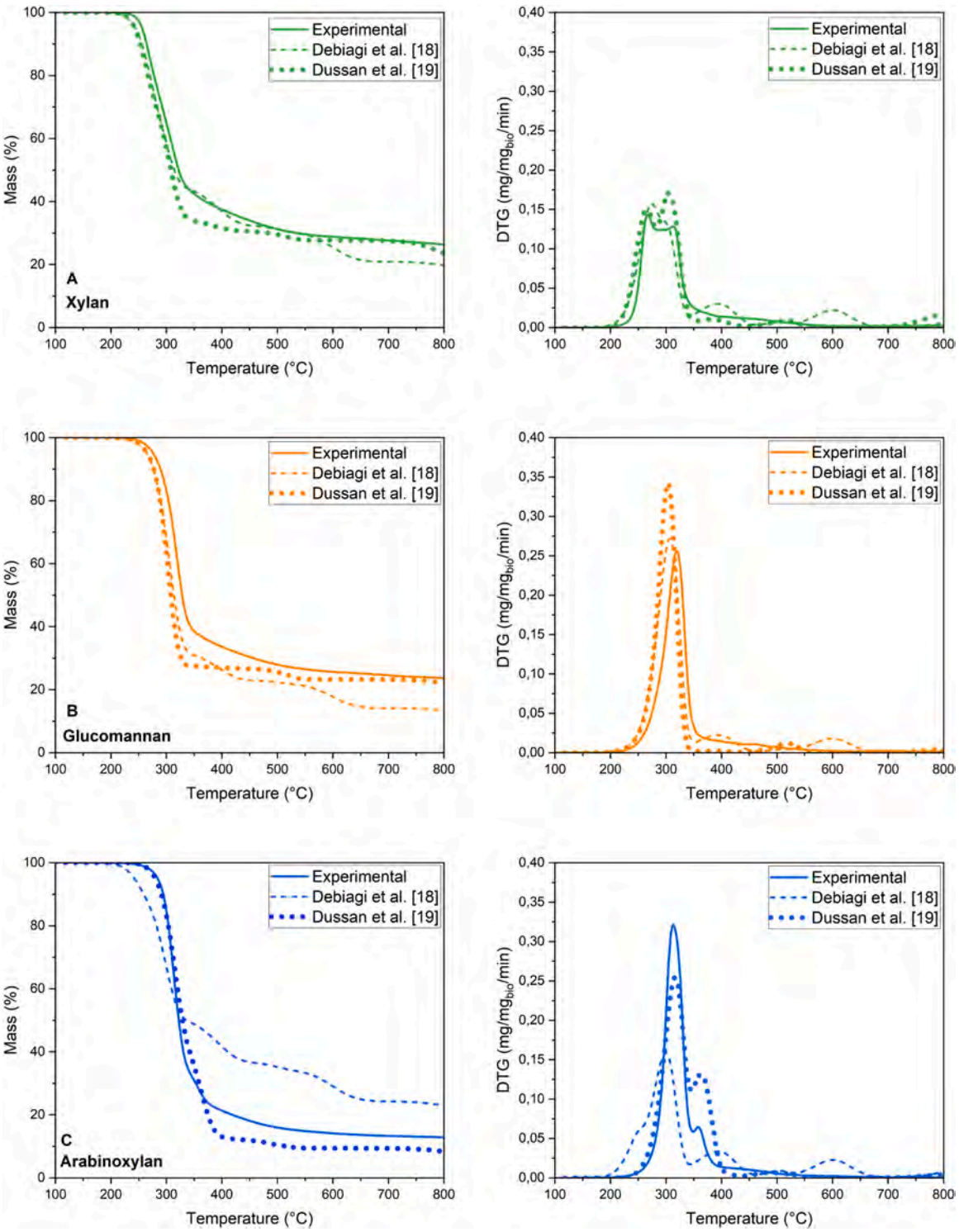

Fig. 9 –. TG and DTG curves for xylan, glucomannan and arabinoxylan at 20 °C/min: comparison between experimental data and model predictions [18,19].

and water yields, underscoring the need for further refinement of kinetic models to improve their predictive accuracy.

To gain deeper insights into the discrepancies observed in the integral yields of broad product categories, a more detailed analysis is performed by comparing the experimental dynamic profiles of water and individual gaseous species with model predictions. Fig. 11 presents the experimental evolution of CO_2, CO, CH_2, and H_2O (left panels) alongside the corresponding predictions by the models of Debiagi et al. [18] (middle panels) and Dussan et al. [19] (right panels) for xylan (A), glucomannan (B), and arabinoxylan (C).

The model by Debiagi et al. [18] significantly underpredicts water production compared to the experimental results of this study, as previously noted in the analysis of integral mass yields. Additionally, it predicts notable gas and water production at temperatures above 350°C, which are either absent or less pronounced in the experimental results. Specifically, the model shows a significant CO_2 peak at 400°C, a contribution of water, CO, and CH_4 around 600°C, and a final release of H_2O and CO at 800°C, which are less evident in the experimental data.

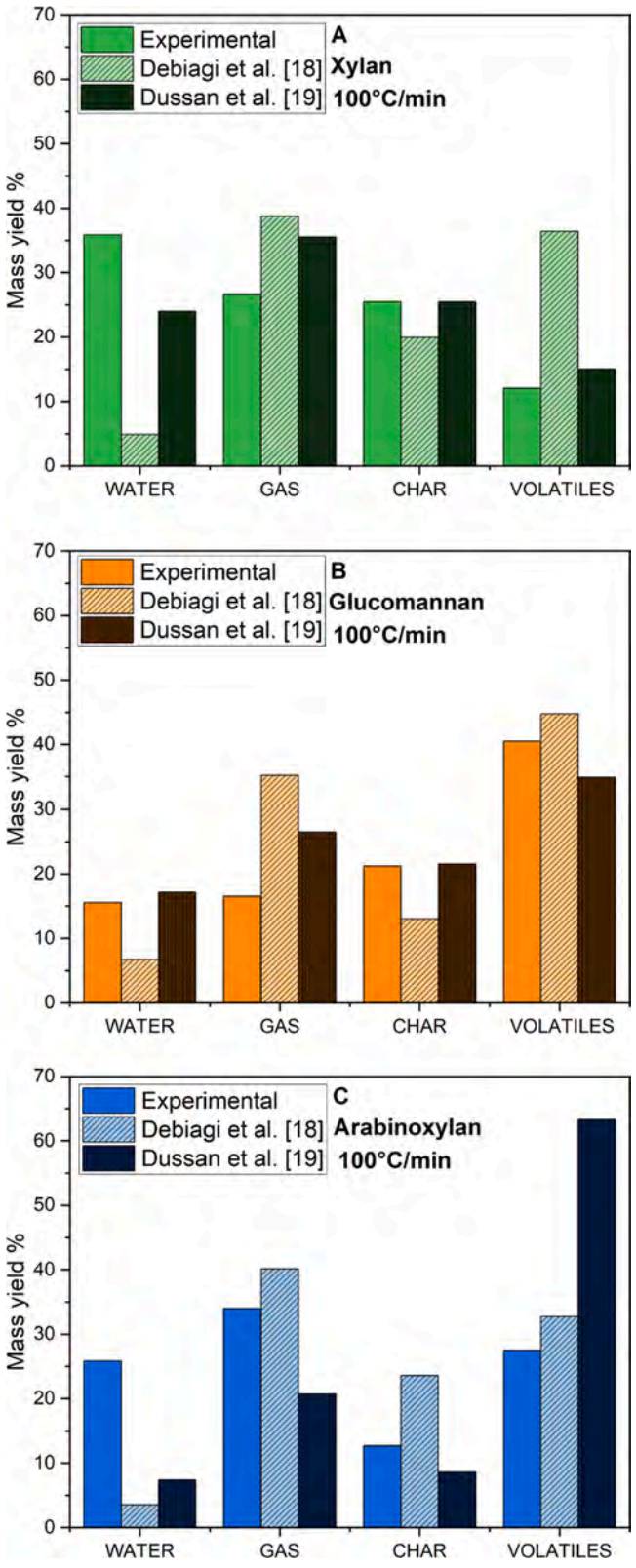

Fig. 10. Integral mass yields of main categories of pyrolysis products for xylan, glucomannan and arabinoxylan at 100 °C/min: comparison between experimental data and model predictions [18,19].

These predicted contributions come from the release of "metaplastic species", which represent lumped intermediates that remain in the solid phase up to higher temperatures before being released into the gas phase as CO_2, CO, CH_4, and H_2O.

The model by Dussan et al. [19] also includes these contributions, even if to a much lesser extent. More importantly however, this model seems to better differentiate the dynamic evolution of gases and water among the various hemicelluloses, more accurately capturing the distinctive behaviors of xylan, glucomannan, and arabinoxylan.

The ability of kinetic schemes to predict bio-oil composition must be also considered. To this purpose, Fig. 12 compares the predicted bio-oil compositions with experimental measurements, revealing significant differences between the two models and the limitations experimental dataset. These discrepancies highlight opportunities for the improvement of these kinetic schemes.

For xylan, the model by Debiagi et al. [18] fails to capture the uniform distribution of products within the C_1–C_9 range, instead predicting a predominance of anhydrosugars and furanic compounds. This diverges from experimental observations, which did not detect anhydrosugars. Conversely, the model by Dussan et al. [19] overestimates the yields of C_2 and C_3 products as well as furanic species. In the case of glucomannan, both experimental data and the predictions from Debiagi et al. [18] indicate a predominance of C_5 and C_6 species, typically associated with anhydrosugars and furanic compounds. However, the model by Dussan et al. [19] fails to include C_5 species in its predictions. Light compounds such as C_1 and C_2 are overestimated by both models, while cyclic oxygenates, which are observed experimentally, are absent in the predicted product distributions. For arabinoxylan the model by Debiagi et al. [18] shows a strong predominance of furanic species, accompanied by a lower production of sugars, ketones and alcohols. Instead, the experimental results show a significantly higher production of sugars and lower presence of furanic species. The model by Dussan et al. [19] well predicts the yields of sugars and furanic species but overestimates the presence of ketones and alcohols.

Overall, this analysis highlights significant gaps in the predictive accuracy of existing models, particularly in capturing the distribution of pyrolysis products. New kinetic models are currently under development based on the comprehensive dataset of this work; in a recent publication, the authors propose a new kinetic scheme developed specifically for glucuronoxylan (the same model molecule herein investigated), overcoming the limitations of the more general models above discussed [47]. Analogous kinetic models for glucomannan and arabinoxylan are currently under development.

4. Conclusions

The development of biomass pyrolysis technologies is constrained by the limited availability of high-quality quantitative data in the literature, making it challenging to establish accurate kinetic models. These models are crucial for designing and optimizing reactors and processes at an industrial scale, enabling more efficient and sustainable biomass conversion.

This study presents an innovative, comprehensive kinetic investigation of hemicellulose pyrolysis, focusing on xylan, glucomannan, and arabinoxylan as representative model compounds for hardwood, softwood, and herbaceous biomass, respectively. A novel TGA-based methodology enabled the simultaneous quantification of devolatilization rates and detailed product speciation, providing a high-quality dataset to refine kinetic models.

Thermogravimetric analyses revealed distinct thermal behaviors among the three hemicelluloses. Xylan underwent a two-step devolatilization, exhibiting the lowest thermal stability, resulting in the highest gas and char yields, and the lowest bio-oil production. Arabinoxylan displayed a dominant primary devolatilization peak followed by a smaller secondary contribution and produced the lowest char yield. In contrast, glucomannan exhibited a single sharp devolatilization peak

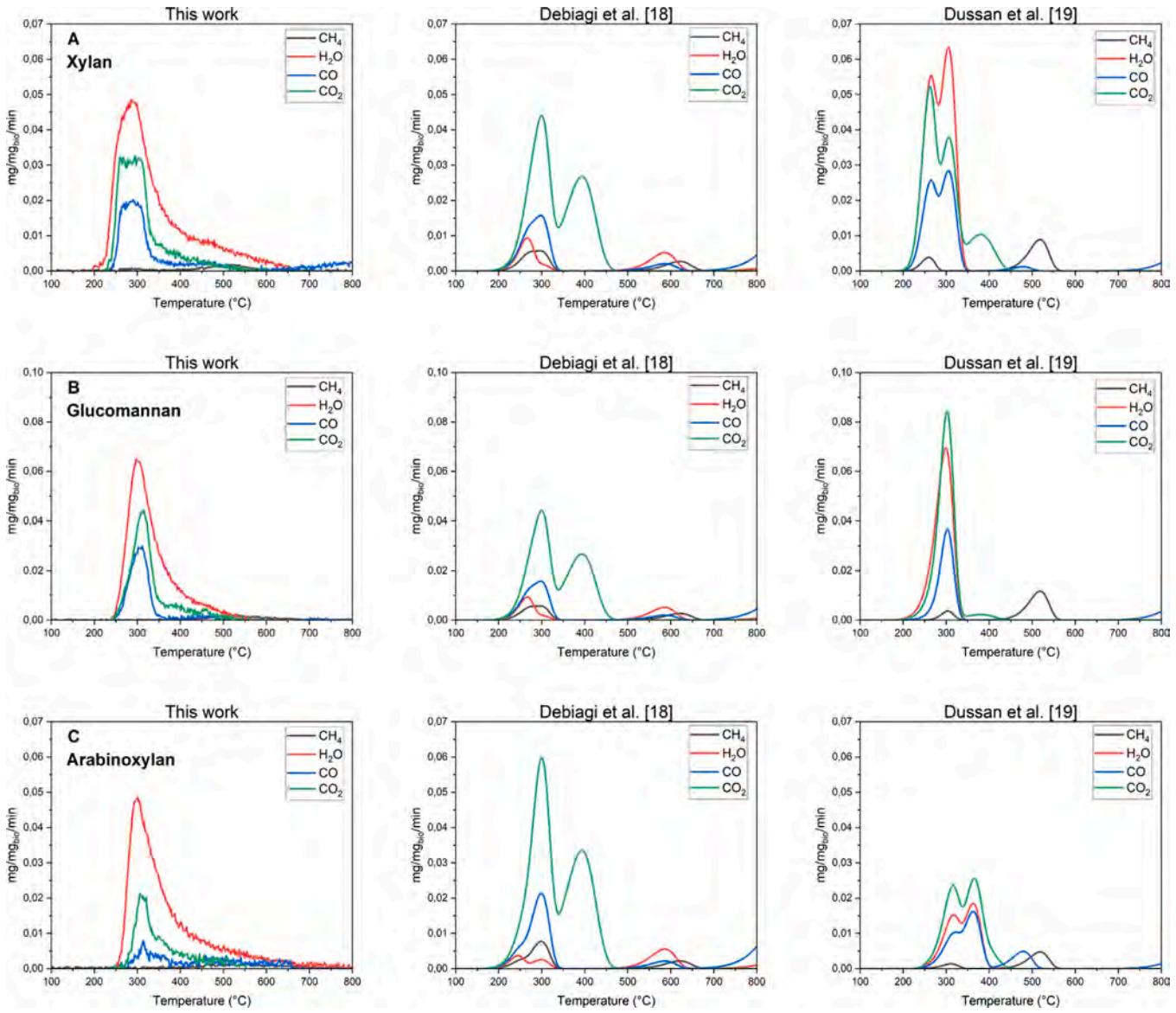

Fig. 11. Comparison of dynamic evolution of gases (CO, CO_2, CH_4) and H_2O for xylan (A), glucomannan (B) and arabinoxylan (C) at 20 °C/min: experimental data and model prediction [18,19].

due to its more ordered structure and lack of lateral substituents, leading to the highest bio-oil yield.

The real-time monitoring of gaseous species provided valuable insights into the dynamic evolution of pyrolysis products. Across all biomasses, the primary devolatilization stage was marked by the release of CO, CO_2, and H_2O. A secondary stage involved CH_4, CO, and residual CO_2, while a tertiary, minor release of CH_4 and CO at higher temperature was likely linked to charring reactions.

Bio-oil analysis unveiled the strong influence of hemicellulose structure on product distribution. Xylan primarily produced aliphatic ketones and furanic species, distributed across the C_1-C_9 range. No anhydrosugars were detected, and specifically, the C_5 anhydrosugar associated with xylan depolymerization, anhydro-xylose, was absent. Glucomannan yielded significant C_6 anhydrosugars, predominantly levoglucosan, indicating substantial monomeric unit release. Arabinoxylan mainly produced C_5 sugars, with dianhydroxylose and 1,4-anhydro-D-xylopyranose as dominant species. Interestingly, the common pentose-based structure of xylan and arabinoxylan yielded very different bio-oil speciation, highlighting a strong influence of the monomeric composition.

Comparison with existing lumped kinetic models showed reasonable predictions for overall mass loss and thermal degradation trends but significant discrepancies in product distribution. Water yield was notably underpredicted, while gaseous species exhibited high-temperature contributions in the models that were absent in the experimental results, due to the delayed release of lumped species in the metaplastic phase. Furthermore, current models fail to represent bio-oil composition, particularly sugar species.

This study highlights the need for improved kinetic parameters and reaction pathways to better capture hemicellulose decomposition complexity. The dataset presented here provides a robust foundation for refining kinetic schemes and enhancing their predictive accuracy for real biomass applications. Future research should integrate these findings into more detailed mechanistic models, expand datasets to include real biomass matrices, and validate model predictions under industrially relevant conditions. Such advancements will be critical for scaling up biomass pyrolysis technologies for biofuel, biochar, and high-value chemical production.

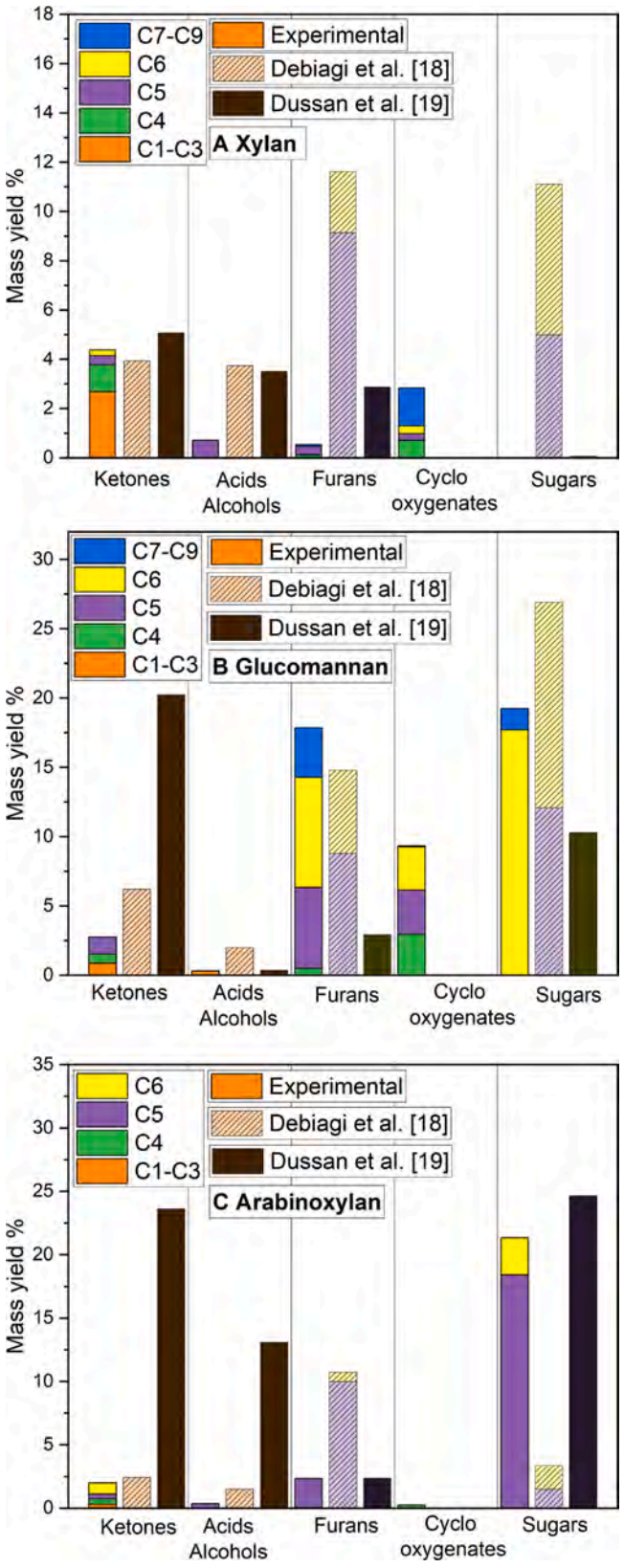

Fig. 12. Bio-oil speciation for xylan, glucomannan and arabinoxylan at 100 °C/min - comparison between experimental data and model predictions [18,19].

CRediT authorship contribution statement

Veronica Piazza: Writing – review & editing, Methodology. **Eleonora Benedetto:** Writing – original draft, Methodology, Investigation. **Alessio Frassoldati:** Writing – review & editing, Supervision. **Luca Lietti:** Writing – review & editing, Supervision, Conceptualization. **Alessandra Beretta:** Writing – review & editing, Supervision, Funding acquisition, Conceptualization. **Tiziano Faravelli:** Writing – review & editing, Supervision.

Declaration of Competing Interest

The authors declare that they have no known competing financial interests or personal relationships that could have appeared to influence the work reported in this paper.

Acknowledgements

This research has received funding from PNRR (PhD scholarship to E. Benedetto). This study was partially conducted within the Agritech National Research Center and received funding from the EU Next-GenerationEU (PNRR) – MISSIONE 4 COMPONENTE 2, INVESTIMENTO 1.4 and 1.3 – D.D. 1032 17/06/2022, CN00000022). This manuscript reflects only the authors' views and opinions, neither the EU nor the EC can be considered responsible for them.

Appendix A. Supporting information

Supplementary data associated with this article can be found in the online version at doi:10.1016/j.jaap.2025.107477.

Data availability

Data will be made available on request.

References

[1] S. Jha, J.A. Okolie, S. Nanda, A.K. Dalai, A review of biomass resources and thermochemical conversion technologies, Chem. Eng. Technol. 45 (2022) 791–799, https://doi.org/10.1002/ceat.202100503.
[2] C.W. Forsberg, B.E. Dale, D.S. Jones, T. Hossain, A.R.C. Morais, L.M. Wendt, Replacing liquid fossil fuels and hydrocarbon chemical feedstocks with liquid biofuels from large-scale nuclear biorefineries, Appl. Energy 298 (2021), https://doi.org/10.1016/j.apenergy.2021.117225.
[3] B. Brehmer, R.M. Boom, J. Sanders, Maximum fossil fuel feedstock replacement potential of petrochemicals via biorefineries, Chem. Eng. Res. Des. 87 (2009) 1103–1119, https://doi.org/10.1016/j.cherd.2009.07.010.
[4] L.A. Lucia, Lignocellulosic biomass: a potential feedstock to replace petroleum, BioResources 3 (2008) 981–982, https://doi.org/10.15376/biores.3.4.981-982.
[5] M.R. Errera, T.A. da, C. Dias, D.M.Y. Maya, E.E.S. Lora, Global bioenergy potentials projections for 2050, Biomass.. Bioenergy 170 (2023), https://doi.org/10.1016/j.biombioe.2023.106721.
[6] E. Ranzi, A. Cuoci, T. Faravelli, A. Frassoldati, G. Migliavacca, S. Pierucci, S. Sommariva, Chemical kinetics of biomass pyrolysis, Energy Fuels 22 (2008) 4292–4300, https://doi.org/10.1021/ef800551t.
[7] I. Energy Agency, Net Zero by 2050 - A Roadmap for the Global Energy Sector, 2050. ⟨www.iea.org/t&c/⟩.
[8] D. Chen, K. Cen, X. Zhuang, Z. Gan, J. Zhou, Y. Zhang, H. Zhang, Insight into biomass pyrolysis mechanism based on cellulose, hemicellulose, and lignin: evolution of volatiles and kinetics, elucidation of reaction pathways, and characterization of gas, biochar and bio-oil, Combust. Flame 242 (2022), https://doi.org/10.1016/j.combustflame.2022.112142.
[9] A.K. Vuppaladadiyam, S.S. Varsha Vuppaladadiyam, V.S. Sikarwar, E. Ahmad, K. K. Pant, M.S., A. Pandey, S. Bhattacharya, A. Sarmah, S.Y. Leu, A critical review on biomass pyrolysis: reaction mechanisms, process modeling and potential challenges, J. Energy Inst. 108 (2023), https://doi.org/10.1016/j.joei.2023.101236.
[10] F.X. Collard, J. Blin, A review on pyrolysis of biomass constituents: mechanisms and composition of the products obtained from the conversion of cellulose, hemicelluloses and lignin, Renew. Sustain. Energy Rev. 38 (2014) 594–608, https://doi.org/10.1016/j.rser.2014.06.013.
[11] X. Zhou, W. Li, R. Mabon, L.J. Broadbelt, A critical review on hemicellulose pyrolysis, Energy Technol. 5 (2017) 52–79, https://doi.org/10.1002/ente.201600327.

[12] J. Rao, Z. Lv, G. Chen, F. Peng, Hemicellulose: structure, chemical modification, and application, Prog. Polym. Sci. 140 (2023), https://doi.org/10.1016/j.progpolymsci.2023.101675.
[13] S. Vikram, P. Rosha, S. Kumar, Recent modeling approaches to biomass pyrolysis: a review, Energy Fuels 35 (2021) 7406–7433, https://doi.org/10.1021/acs.energyfuels.1c00251.
[14] S. Hameed, A. Sharma, V. Pareek, H. Wu, Y. Yu, A review on biomass pyrolysis models: Kinetic, network and mechanistic models, Biomass.. Bioenergy 123 (2019) 104–122, https://doi.org/10.1016/j.biombioe.2019.02.008.
[15] G. Navarrete Cereijo, P. Galione Klot, P. Curto-Risso, Two-stage global biomass pyrolysis model for combustion applications: predicting product composition with a focus on kinetics, energy, and mass balances consistency, Energies 17 (2024), https://doi.org/10.3390/en17194982.
[16] Y. Haseli, J.A. Van Oijen, L.P.H. De Goey, Modeling biomass particle pyrolysis with temperature-dependent heat of reactions, J. Anal. Appl. Pyrolysis 90 (2011) 140–154, https://doi.org/10.1016/j.jaap.2010.11.006.
[17] S. Niksa, bio-FLASHCHAIN® theory for rapid devolatilization of biomass. 8. Validations for hardwoods, J. Anal. Appl. Pyrolysis 175 (2023), https://doi.org/10.1016/j.jaap.2023.106202.
[18] P. Debiagi, G. Gentile, A. Cuoci, A. Frassoldati, E. Ranzi, T. Faravelli, A predictive model of biochar formation and characterization, J. Anal. Appl. Pyrolysis 134 (2018) 326–335, https://doi.org/10.1016/j.jaap.2018.06.022.
[19] K. Dussan, S. Dooley, R. Monaghan, Integrating compositional features in model compounds for a kinetic mechanism of hemicellulose pyrolysis, Chem. Eng. J. 328 (2017) 943–961, https://doi.org/10.1016/J.CEJ.2017.07.089.
[20] T. Faravelli, A. Frassoldati, G. Migliavacca, E. Ranzi, Detailed kinetic modeling of the thermal degradation of lignins, Biomass.. Bioenergy 34 (2010) 290–301, https://doi.org/10.1016/j.biombioe.2009.10.018.
[21] E. Ranzi, M. Corbetta, F. Manenti, S. Pierucci, Kinetic modeling of the thermal degradation and combustion of biomass, Chem. Eng. Sci. 110 (2014) 2–12, https://doi.org/10.1016/j.ces.2013.08.014.
[22] E. Ranzi, P.E.A. Debiagi, A. Frassoldati, Mathematical modeling of fast biomass pyrolysis and bio-oil formation. note i: kinetic mechanism of biomass pyrolysis, ACS Sustain Chem. Eng. 5 (2017) 2867–2881, https://doi.org/10.1021/acssuschemeng.6b03096.
[23] R. Moriana, Y. Zhang, P. Mischnick, J. Li, M. Ek, Thermal degradation behavior and kinetic analysis of spruce glucomannan and its methylated derivatives, Carbohydr. Polym. 106 (2014) 60–70, https://doi.org/10.1016/j.carbpol.2014.01.086.
[24] G. Dai, G. Wang, K. Wang, Z. Zhou, S. Wang, Mechanism study of hemicellulose pyrolysis by combining in-situ DRIFT, TGA-PIMS and theoretical calculation, in: Proceedings of the Combustion Institute, Elsevier Ltd, 2021, pp. 4241–4249, https://doi.org/10.1016/j.proci.2020.06.196.
[25] V. Piazza, R.B. da Silva Junior, A. Frassoldati, L. Lietti, S. Chiaberge, C. Gambaro, A. Siviero, T. Faravelli, A. Beretta, Detailed speciation of biomass pyrolysis products with a novel TGA-based methodology: the case-study of cellulose, J. Anal. Appl. Pyrolysis 178 (2024), https://doi.org/10.1016/j.jaap.2024.106413.
[26] V. Piazza, R. Batista da Silva Junior, A. Frassoldati, L. Lietti, C. Gambaro, K. Rajendran, D. Chen, T. Faravelli, A. Beretta, Unravelling the complexity of hemicellulose pyrolysis: Quantitative and detailed product speciation for xylan and glucomannan in TGA and fixed bed reactor, Chem. Eng. J. 497 (2024) 154579, https://doi.org/10.1016/J.CEJ.2024.154579.
[27] N. Worasuwannarak, T. Sonobe, W. Tanthapanichakoon, Pyrolysis behaviors of rice straw, rice husk, and corncob by TG-MS technique, J. Anal. Appl. Pyrolysis 78 (2007) 265–271, https://doi.org/10.1016/j.jaap.2006.08.002.
[28] K. Werner, L. Pommer, M. Broström, Thermal decomposition of hemicelluloses, J. Anal. Appl. Pyrolysis 110 (2014) 130–137, https://doi.org/10.1016/j.jaap.2014.08.013.
[29] D.K. Shen, S. Gu, A.V. Bridgwater, Study on the pyrolytic behaviour of xylan-based hemicellulose using TG-FTIR and Py-GC-FTIR, J. Anal. Appl. Pyrolysis 87 (2010) 199–206, https://doi.org/10.1016/j.jaap.2009.12.001.
[30] S. Niksa, On the primary devolatilization of hemicellulose, J. Anal. Appl. Pyrolysis 164 (2022), https://doi.org/10.1016/j.jaap.2022.105515.
[31] S. Wang, B. Ru, H. Lin, Z. Luo, Degradation mechanism of monosaccharides and xylan under pyrolytic conditions with theoretic modeling on the energy profiles, Bioresour. Technol. 143 (2013) 378–383, https://doi.org/10.1016/j.biortech.2013.06.026.
[32] M. Ghalibaf, T.R.K.C. Doddapaneni, R. Alén, Pyrolytic behavior of lignocellulosic-based polysaccharides, J. Therm. Anal. Calor. 137 (2019) 121–131, https://doi.org/10.1007/s10973-018-7919-y.
[33] C. Branca, C. Di Blasi, C. Mango, I. Hrablay, Products and kinetics of glucomannan pyrolysis, Ind. Eng. Chem. Res. 52 (2013) 5030–5039, https://doi.org/10.1021/ie400155x.
[34] P.R. Patwardhan, R.C. Brown, B.H. Shanks, Product distribution from the fast pyrolysis of hemicellulose, ChemSusChem 4 (2011) 636–643, https://doi.org/10.1002/cssc.201000425.
[35] W.T. Tsai, M.K. Lee, Y.M. Chang, Fast pyrolysis of rice husk: product yields and compositions, Bioresour. Technol. 98 (2007) 22–28, https://doi.org/10.1016/j.biortech.2005.12.005.
[36] P. Debiagi, V. Piazza, M. Papagni, A. Beretta, A. Frassoldati, T. Faravelli, Cellulose pyrolysis kinetic model: detailed description of volatile species, Proc. Combust. Inst. 40 (2024), https://doi.org/10.1016/j.proci.2024.105651.
[37] S. Wang, G. Dai, H. Yang, Z. Luo, Lignocellulosic biomass pyrolysis mechanism: a state-of-the-art review, Prog. Energy Combust. Sci. 62 (2017) 33–86, https://doi.org/10.1016/j.pecs.2017.05.004.
[38] P. Pariyar, K. Kumari, M.K. Jain, P.S. Jadhao, Evaluation of change in biochar properties derived from different feedstock and pyrolysis temperature for environmental and agricultural application, Sci. Total Environ. 713 (2020), https://doi.org/10.1016/j.scitotenv.2019.136433.
[39] D. Magalhães, K. Gürel, L. Matsakas, P. Christakopoulos, I. Pisano, J.J. Leahy, F. Kazanç, A. Trubetskaya, Prediction of yields and composition of char from fast pyrolysis of commercial lignocellulosic materials, organosolv fractionated and torrefied olive stones, Fuel 289 (2021), https://doi.org/10.1016/j.fuel.2020.119862.
[40] Z. Dong, Y. Wei, Y. Chen, L. Zhang, D. Xu, G. Lin, Bin Li, S. Zhang, J. Wei, M. A. Akhtar, J. Sun, Nitrogen migration and transformation in chars and tars during co-pyrolysis of cellulose/xylan/lignin with urea formaldehyde, J. Anal. Appl. Pyrolysis 178 (2024), https://doi.org/10.1016/j.jaap.2024.106425.
[41] M.W. Smith, B. Pecha, G. Helms, L. Scudiero, M. Garcia-Perez, Chemical and morphological evaluation of chars produced from primary biomass constituents: cellulose, xylan, and lignin, Biomass.. Bioenergy 104 (2017) 17–35, https://doi.org/10.1016/j.biombioe.2017.05.015.
[42] Z. Ma, Y. Yang, Y. Wu, J. Xu, H. Peng, X. Liu, W. Zhang, S. Wang, In-depth comparison of the physicochemical characteristics of bio-char derived from biomass pseudo components: Hemicellulose, cellulose, and lignin, J. Anal. Appl. Pyrolysis 140 (2019) 195–204, https://doi.org/10.1016/j.jaap.2019.03.015.
[43] K.B. Ansari, J.S. Arora, J.W. Chew, P.J. Dauenhauer, S.H. Mushrif, Fast pyrolysis of cellulose, hemicellulose, and lignin: effect of operating temperature on bio-oil yield and composition and insights into the intrinsic pyrolysis chemistry, Ind. Eng. Chem. Res 58 (2019) 15838–15852, https://doi.org/10.1021/acs.iecr.9b00920.
[44] D. Sangaré, V. Belandria, S. Bostyn, M. Moscosa-Santillan, I. Gökalp, Pyro-gasification of lignocellulosic biomass: online quantification of gas evolution with temperature, effects of heating rate, and stoichiometric ratio, Biomass.. Convers. Biorefin 14 (2024) 9763–9775, https://doi.org/10.1007/s13399-022-03103-x.
[45] B. Hu, Q. Lu, Z.X. Zhang, Y.T. Wu, K. Li, C.Q. Dong, Y.P. Yang, Mechanism insight into the fast pyrolysis of xylose, xylobiose and xylan by combined theoretical and experimental approaches, Combust. Flame 206 (2019) 177–188, https://doi.org/10.1016/j.combustflame.2019.04.052.
[46] J. Duan, H. Hu, J. Ji, Mechanism study on arabinose pyrolysis by combining TG-FTIR-GC–MS and theoretical calculations, Combust. Flame 245 (2022), https://doi.org/10.1016/j.combustflame.2022.112352.
[47] M.Y. Suleiman, E. Benedetto, V. Piazza, L. Lietti, A. Frassoldati, T. Faravelli, A. Beretta, P. Debiagi, Kinetic modelling of biomass pyrolysis: a new lumped scheme for xylan-based hardwood hemicellulose, Energy Convers. Manag. X (2025) 101130, https://doi.org/10.1016/j.ecmx.2025.101130.